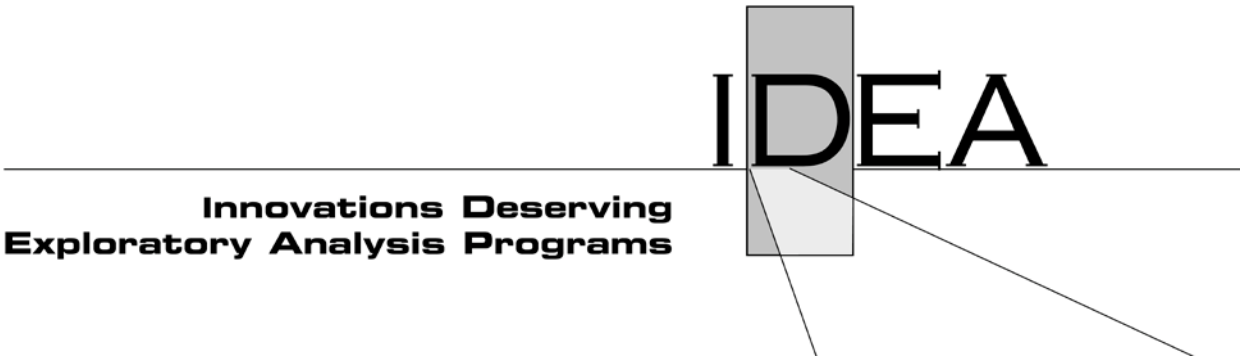

NCHRP IDEA Program

A Class of V-Connectors for Bridge Deck-Pier and Pier-Footing Joints with the Combined Advantage of Integrated Design and Seismic Isolation while Enabling Accelerated Bridge Construction

Final Report for
NCHRP IDEA Project 188

Prepared by:
Su Hao, Ph.D.
ACII, Inc.

March 2018

TRB TRANSPORTATION RESEARCH BOARD
The National Academies of
SCIENCES · ENGINEERING · MEDICINE

A Class of V-Connectors for Bridge Deck-Pier and Pier-Footing Joints with the Combined Advantage of Integrated Design and Seismic Isolation while Enabling Accelerated Bridge Construction

IDEA Program Final Report

NCHRP IDEA Project 188

Prepared for the IDEA Program
Transportation Research Board
The National Academies of Sciences, Engineering and Medicine

Su Hao, Ph.D.
ACII, Inc.
Irvine, California

March 31, 2018

Table of Contents

List of Figures and Tables

Figures

Tables

Glossary of Terms and Symbols

Δ, Δ_{sub}, Δ_{iao}, Δ_{total}: Displacement, lateral displacement of substructure, lateral displacement of isolator, and total lateral displacement, respectively
E, E_C, E_S: Young's modulus, Young's modulus of concrete, and Young's modulus of steel, respectively
ϕ_v, ϕ_p: Diameters of the V-guiding tube's (VGT's) opening and the part to hold pin, respectively
$f(x)$: Curvature of VGT
f_c', $f_{fracture}$: Compressive and tensile strengths of concrete, respectively
$F_{failure}$: Failure load of the V-connector
F_{PGA}, F_a, F_v: the site scale factors for zero, short, and long period range of accelerated spectrum, respectively
H_v: Height of V-connector for lateral displacement that equals its crater's depth L_c
H_{sub}: Height of substructure
K, K_{eff}: Stiffness and Effective stiffness
f_r: Friction coefficient
I: Sectional bending moment
K_d: Post-elastic stiffness on hysteresis loop
K_V: Elastic stiffness of V-connector that is mainly contributed by the stabilization pin (SBP)
$\lambda_t(x)$: Radius of the SBP
L_t: Length of a VGT's part to hold the pin (SBP)
L_c: Length of a VGT's part with V-shaped crater
P: Load
P_e: Yield load of substructure
PGA: Peak ground Acceleration
Q, Q_d: Shear force and characteristic strength, see the definition in [7-9]
ρ_S, ρ_C: Density of steel and concrete, respectively
R: Ductility factor
S_S, S_1: Spectrum acceleration coefficient at 0.2 and 1 seconds, respectively,
S_{DS}, S_{D1}: $S_{DS} = F_a S_S$ and SD1 $= F_v S_1$
σ_Y, σ_u: Yield and ultimate strength
W_{sup}: Weight of superstructure
ξ: equivalent damping ratio

Acknowledgements

The principal investigator (P.I.) of this project expresses his sincere appreciation to Dr. Inam Jawed, the TRB IDEA Program Manager for the part of sponsored research described in this report. Without his mentoring and advising in both project management and scientific research, this project would not have been completed. The P.I. also sincerely thanks Mr. Joseph Horton, project advisor on the behalf of the IDEA program, for his support and guidance during the course of the project. Thanks are also due to the IDEA review committee for providing valuable comments on the draft of this report.

The P.I. also expresses his sincere appreciation to his collaborators -- Professor Khalid Mosalam, Director, Pacific Earthquake Engineering Research (PEER) Center at the University of California at Berkeley; Dr. Shakhzod Takhirov, Manager, PEER Center Laboratory; Mr. Yingjie Wu, Ph. D. student; and Dr. Selim Gunay, postdoctoral fellow at the PEER -- for their tireless efforts and help in conducting the V-connector tests. Special thanks are also due to Professor Shaofan Li, and Professor Claudia Ostertag, Department of Civil and Environmental Engineering, University of California at Berkeley for their kind support and the late Professor Stephen Mahin, Past Director, PEER Center, for his valuable advice.

The P.I. also thanks Mr. Guang-En Song, General Manager, and Mr. Ruixiang Xu and Mr. Jun Li, research engineers, Fengzhe Intelligent Equipment Company, Ltd. (formerly Fengzhe Engineering Rubber Technological Development Company. Ltd.) in China for their assistance in manufacturing and testing the V-connectors in their laboratory.

The P.I. also would like to thank Mr. Richard Pratt, State Bridge Engineer, Alaska DOT, Mr. Bijan Khaleghi, State Design Engineer, and Mr. Thomas Baker, Washington State DOT, Mr. Thomas Ostrom, State Bridge Engineer, and Mr. Don Li, Caltrans, Mr. Wayne Seger, Director, Structures Division (retired), Tennessee DOT, and Professor Bojidar Yanev of Columbia University and New York City DOT for their helpful discussions and support.

Finally, the P.I. expresses his gratitude to Mr. Ronald Watson, President, R.J. Watson, Inc., for his continued support in the development of the V-connectors and his staff for their assistance in fabricating the V-connectors tested in this research.

Executive Summary

A long-existing challenge to the bridge engineering community is how to achieve fast construction while ensuring a structure's integrity and sustainability. In a densely populated area, building a bridge may take a long time, often causing traffic congestion that results in not only inconvenience to the motoring public but also economic losses due to unproductive time lost in traffic delays. Technologies and methods for accelerating construction are certainly desirable or necessary but only if structural integrity and robustness of the structure are assured for public safety. To simultaneously meet these rather competing needs is crucial, particularly when constructing structures in high seismic risk areas. The objective of this NCHRP-IDEA research was to develop a technology based on an innovative class of joint products, termed, V-connectors, to address the requirements of both accelerated construction and the safety and seismic resistance for bridge structures.

The V-connector is an innovative joint device that can be used to connect any two construction elements in a structural system, for example, as a weight-carrying bearing between a bridge pier and its span, or a pier and its foundation. A V-connector assures robust connection while allowing relative sliding motion between the contact surface of the two connected elements, which helps reduce the system's vibration and causes phase shift in its natural frequencies to avoid possible resonance. By employing a specially-designed V-shaped geometry, the connector keeps the relative sliding motion smooth with gradually-increasing resistance to further sliding, which produces the needed ductility for seismic isolation.

The design of the V-connector ensures that all connected elements always stay in elastic condition. However, when an earthquake strikes, it exhibits a reversible "ductile" hysteresis behavior in the lateral force vs. sliding displacement correlation curve for the structural system due to the relative sliding. Such a ductile behavior is a key characteristic for a seismic-resistant bearing. Since the entire structural system would remain in elastic condition, the bearing would be able to restore the bridge to its original state after the earthquake passes. In addition to the needed seismic resistance and the self-restoration capability, the V-connector provides integrity and robustness to a bridge similar to those of a cast-in-place (CIP) bridge as well as the capability for accelerated bridge construction (ABC). The ABC capability also applies to modular bridges in which parts, pre-fabricated in a factory elsewhere, are brought and assembled on-site in about a day.

The concept of the V-connector, the predicted hysteresis behavior, and other aforementioned anticipated advantages were investigated in this two-stage research. In the first stage, the effects of the connector's design parameters on the requirements of structural robustness, seismic isolation, and fast construction were studied. The objective was to optimize the design parameters, based on the analysis of theoretical modeling and 2D and 3D finite element (FE) simulations (Fig. A1). Work in the second stage involved verification and validation of the performance of the developed connector system. Two sets of V-connectors were designed to meet the requirements of a benchmark highway bridge example (provided in the AASHTO LRFD manual) and a railroad bridge example. The connectors were manufactured and tested at the Pacific Earthquake Engineering Research (PEER) Center Laboratory of the University of California at Berkeley and the Fengzhe Laboratory in China. The test results from both laboratories verified the anticipated advantages of the V-connectors and validated their applicability for seismic isolation (Figs. A2 and A3). Design-diagrams for the family of V-connectors were produced (Fig. A4), which can be used to guide the design of V-connectors in accordance with practical conditions of actual bridges.

Several State DOTs have shown interest in this sponsored research. The product, when implemented after further evaluation and validation, is expected to have a high pay-off potential for bridge structures in terms of providing structural robustness, seismic protection, ease of maintenance, capability for fast construction, and the associated economic benefits.

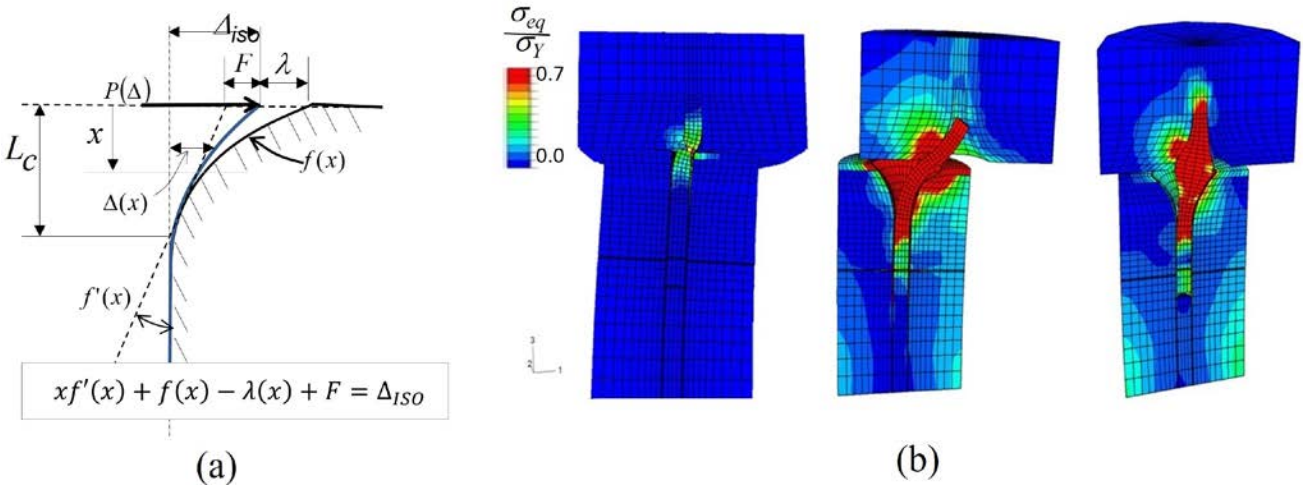

Fig. A1（a）Theoretical model and derived governing differential equation of V-connector; (b) examples of 3D FE simulations

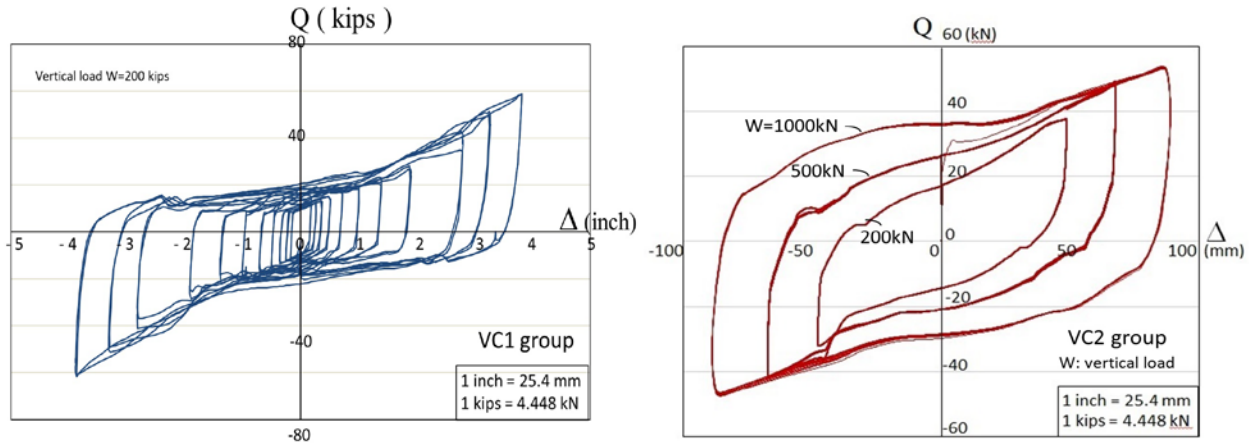

Fig. A2. Measured hysteresis behaviors for the tests at UC Berkeley (left) and Fenzhe Lab. of China (right)

Fig. A3. Testing at the PEER lab of UC Berkeley

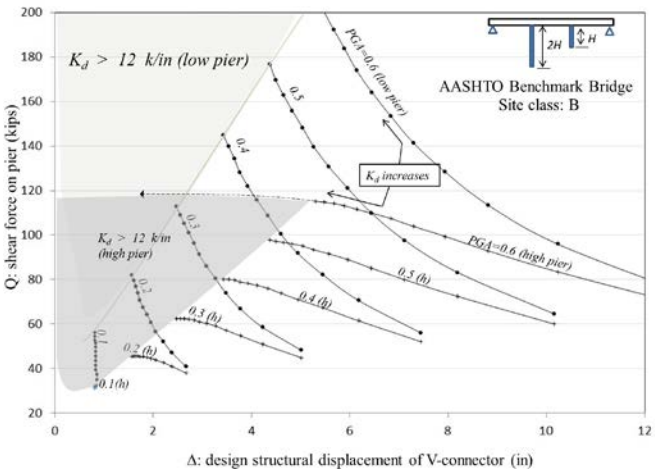

Fig. A4. Design diagram of the V-connector for bridges with uneven piles heights.

1. IDEA Product and Rationale

A 2015 United States Geological Survey report [2] with an updated forecast for future earthquakes along the San Andreas Fault that stretches along the State of California has predicted a 20% increase in the probability of earthquakes with magnitudes of eight or higher within the next 30 years. This implies that, on the West Coast of the United States, the risk of devastating events like the earthquakes in Chile in 2009 and Japan in 2011 is higher than that previously expected. The 2011 Virginia earthquake served as a wake-up call that the East Coast too was not immune to seismic threats. Although the epicenter for that 5.8 magnitude Virginia earthquake was about 100 miles away from Washington DC, there was damage to structures in the city. For example, cracks appeared in the Washington Monument and one of the National Cathedral's towers lost its tip. The induced shock-waves were felt as far away as New England. In Pennsylvania, there were observable structural movements at a nuclear power plant.

Along with efforts to prevent future earthquake damage to bridges and buildings in high seismic regions of the United States, accelerated construction and rapid retrofit are also the current needs of the bridge engineering industry. A Texas DOT-sponsored research [3] estimated an economic loss of about $78 billion per year due to traffic congestion nationwide, a significant portion of which was attributed to bridge construction, repair, and replacement work. From the viewpoint of disaster resilience, the capability of rapid construction and retrofit/replacement of a damaged life-line bridge will allow quick restoration of normal life and economic activity. To these ends, the challenge is to design and build structures with sufficient robustness to sustain future earthquakes and doing it in a most economical way in the least amount of time and also striving to make them require minimum maintenance, repair, or replacement efforts.

To address the above challenge, this NCHRP IDEA-sponsored research was aimed at developing a class of innovative structural connectors, termed, V-connector [4-6], that could be used to join two major structural parts of a bridge or a building, for example, as a seismic isolation bearing connecting the superstructure and pier of a bridge. Specifically, the goal of this project was to investigate and establish the following features of the developed innovative V-connectors:

(A) Robustness – a stable connection under normal operating conditions
(B) Fuser – capable of accommodating temporal separation between two connected parts of a structure when one of them is dragged by a sudden accelerated motion, such as when a bridge pier is impacted by earthquake, barge or vessel collision, explosion, etc. Such a separation would substantially reduce the transfer of inertia-induced forces to another part and cause a shift in the bridge's natural frequencies to avoid vibration resonance
(C) Self-healing – capable of self-restoring the structure to its original state after an impact load
(D) Integrity – capable of keeping the two connected parts as an integrated system during temporal separation; in other words, this separation should not result in a permanent detachment, which is particularly important for situations like when a bridge superstructure is struck by an impact
(E) Environment-friendly – should not introduce noise or extra material hazards nor consume extra energy
(F) Convenience for long-term maintenance – the components of a V-connector should be designed and fabricated to last at least as long as the rebars in concrete would.
(G) Easy for erection and other related construction work, enabling accelerated construction
(H) Cost-effective by providing benefits of ABC, seismic-resistance, and maintenance convenience.

A basic function of a seismic-resistant bearing for a bridge is to introduce "ductility" to the structural system. When an earthquake-induced ground motion hits a bridge substructure beneath the bearing, it allows a temporal separation between the substructure and the superstructure. Additionally, the relationship between the force acting on the superstructure and the separation-induced displacement presents a nonlinear condition when the load is high. According to design codes [7-9], only horizontal separation (sliding) is to be considered in the current engineering design. This practice is also followed in this report. The design of a V-connector is such that it keeps all involved structural parts in elastic condition when an earthquake strikes a structure, for which the ductility is produced by the nonlinearity between the internal friction force and the sliding displacement. This sliding motion-friction also allows energy dissipation. The allowance of this separation and the associated capacity to dissipate energy are quantitatively represented by the parameter ξ, termed, equivalent damping ratio [7-9]. ξ is proportional to the energy dissipated during each vibration cycle. As compared to conventional seismic isolation bearings, **the benchmark properties of the developed V-connectors are:**

1) **High ductility and high equivalent damping ratio while structural components remain in elastic condition**
2) **Self-restoration capability**
3) **As a load-carrying bearing, high load capacity based on a simple mechanical design**

4) **Structural integrity and robustness similar to those of CIP concrete structure, while enabling ABC**
5) **No extra requirements for the structure's geometry, such as an enlarged pier seat or cantilever abutment**
6) **Convenient for maintenance**

Two sets of V-connector products were designed for a highway bridge (Fig. 1a), recommended by the AASHTO Bridges and Structures Subcommittee's T3 Technical Committee (Bridge Seismic Design), and a railway bridge (Fig. 1b). The connector specimens were manufactured and tested to verify the above-listed key properties at the PEER Center Laboratory at the University of California at Berkeley and the Fengzhe Laboratory in China.

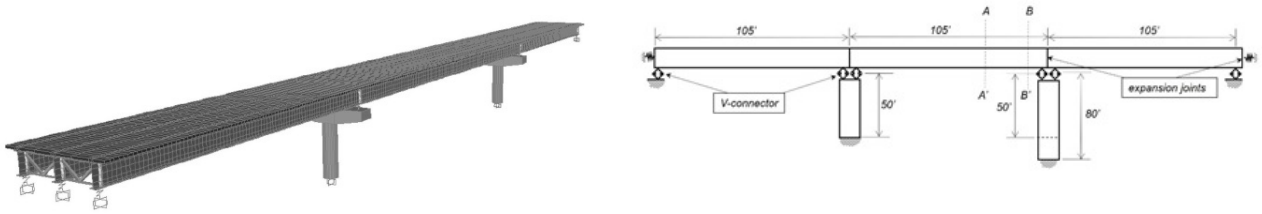

(a) AASHTO benchmark highway bridge [7-9] (b) A design example of a railway bridge

Fig. 1: Benchmark bridges as application examples for the V-connector system

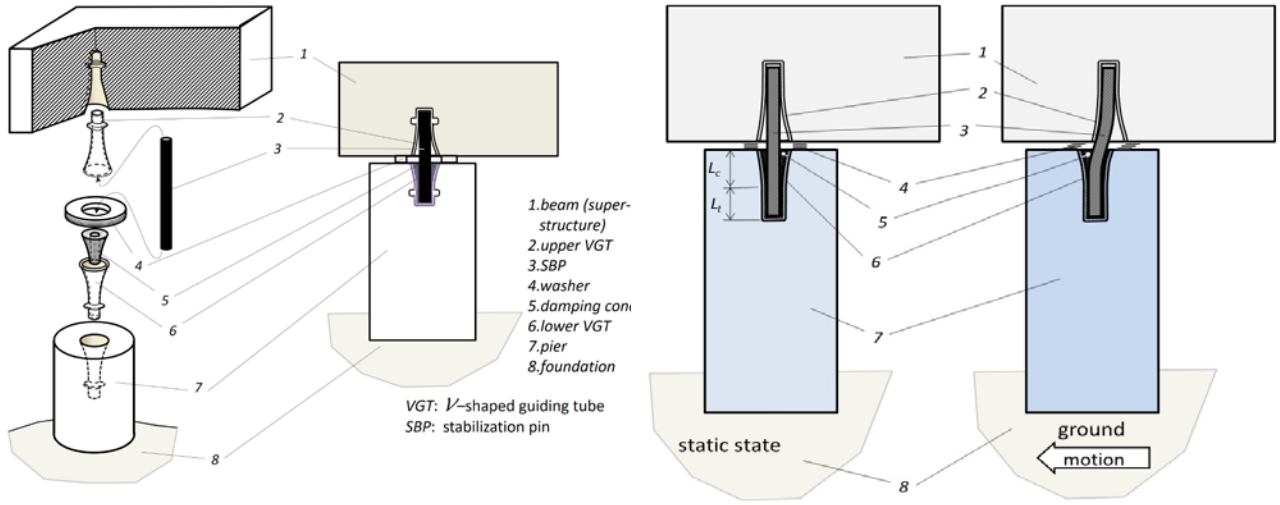

(a) (b)

Fig. 2. Conceptual illustrations of the V-connector: (a) basic structure and components; (b) design of VGT that comprises two parts, where the first part of length L_t is with the inner geometry and size that are the same as the outer geometry and size of the pin, the second part of length L_C is with a V-shaped crater.

2. Concept and Innovation

The basic concept of a V-connector is illustrated by the configurations in Figs. 2a and 2b, which is an assembly of five basic elements installed between two connected parts of a structure (bridge deck and pier in the figure) -- two V-shaped guiding tubes (abbreviated as VGT), a vertical stabilizing pin (abbreviated as SBP) with its two ends inserted into the two VGTs, a damping cone around the pin within the lower VGT, and a washer. While serving as a seal to prevent dirt from falling into the VGT, the major function of the washer is to provide friction-induced energy dissipation when an earthquake strikes a bridge. The damping cone is an optional accessory, which is inserted within the crater-shaped part of the lower VGT around the pin.

Using a pin to connect two structural parts and restrict lateral relative motion between those parts is a common engineering practice. For a structure with seismic resistance requirement, pins (such as the conventional shear key) are often employed to reinforce the structural integrity. To the best of the author's knowledge, for all pin-like connectors used so far in bridges and buildings, either the two end parts of the pin are embedded into two cylindrical holes on each of the two connected structural parts (termed, two-end fixed pin-connector, in this report) or the pin is designed to be sacrificed for permanent ductile deformation and failure to reduce impact when struck by an earthquake, for example, like a shear key. Though these kinds of pins provide robust connection, the two-end fixed pin-connector lacks the ductility needed for seismic isolation while the shear key cannot restore the structure to its original state after the impact load passes. In both cases, localized high bending moment and shear stress occur in the pin, and super-high localized compression stress is exerted on the edges of the connected concrete parts. When these types of pin connectors are used to connect a long span and two piers, extra requirements are needed to fit construction tolerance and accommodate the span's thermal expansion or shrinkage, which makes accelerated construction rather impractical.

The primary innovation of the V-connector is the design of a V-shaped cavity for the VGT with the following five functions:

(i) Introduces flexibility as a conventional isolation bearing that allows relative separation between the super- and substructures when an earthquake strikes;
(ii) Accommodates manufacture tolerance and thermally-induced deformation of the superstructure, leading to fast assembly capability for bridge erection, i.e. enabling ABC;
(iii) Ensures sustainability by significantly reducing stress concentration on the edges of the concrete pier and beam caused by the pin when the system is under high dynamic load;
(iv) Allows SBP design with various sizes and geometries so that a combination of SBP-VGT could assure that the SBP would not be cut by shear force under extremely high applied dynamic load and the system would have the robustness of the CIP concrete system; and
(v) Enhances capacity to allow self-restoration of the system.

The following is a discussion of how these functions can be achieved by the V-connector.

A VGT has two parts along its longitudinal direction, characterized by different geometries (Fig. 2b). The first part is a V-shaped crater with length L_C while the second part has a cylinder-like geometry of length L_t. This second part has the same inner geometry and size as the SBP's outer geometry and size, which allows inserting the pin snugly into this part. This establishes a robust connection without relative motion along the horizontal direction when L_t is long enough and the pin is made of a material of sufficient strength; there is, however, no restriction along the vertical direction. The V-shaped cavity of the VGT helps guide the insertion of the SBP, which facilitates the joining of the two structural blocks with the added advantage of fast construction.

The SBP is able to bend within the V-shaped crater of the VGT when relative sliding motion occurs along the contact surface of the two blocks and its end is held tightly by the VGT part of length L_t. This imparts seismic isolation capability to the connector. Consider, for example, a bridge in which the superstructure is connected to the pier top through a V-connector (Fig. 2b). When the pier is struck by a dynamic load, there is a relative motion between the two connected blocks along both vertical and horizontal directions. With the inserted SBP, the VGT part of length L_t guides the vertical separation and assures no loss of connection if the separation is less than half the length of the SBP. For horizontal motion, the V-shaped crater part of the VGT that has a specially-designed internal curvature allows the pin, when it bends, to contact this VGT part's inner wall asymptotically, which produces gradually elevating lateral resistance and results in a reversible contact-induced nonlinearity that presents as the curve between the bending-induced lateral force and the horizontal deflection, depicted in Fig. 3a. The relationship between this horizontal deflection and the friction force on the contact surface of the two blocks presents as the hysteresis loops shown in Fig. 3b during vibration cycles. A combination of the curves in Figs. 3a and 3b is the predicted hysteresis curve, shown in Fig. 3c, for a V-connector, which is exactly what is required for seismic isolation. By employing the design method described later, the SBP can be ensured to always remain within the elastic condition and provide the needed driving force for self-restoration.

When a pin is used for connection, the most common failure pattern is that the pin is cut by shear stress concentration. The V-connector avoids this failure risk because of its two particular features. First, it has the flexibility to enlarge the SBP's diameter within the V-shaped crater part of the VGT where the shear stress may be higher or to add a shear reinforcement ring, termed, V-ring (SRV), on this part of SBP, as shown in Fig. 4. Second, when relative-sliding between two connected structural parts becomes significant, the accompanying shear force acting on the SBP introduces gradually-increasing compression over the area where the SBP's circumferential surface contacts with the VGT's inner

wall instead of localized shear stress, if the geometries of the SBP-VGT pair are appropriately designed. This mechanism was verified by numerical simulations and experiments carried out in this research.

Geometry-wise, there is no substantial difference between the upper and lower VGTs of the V-connectors (Figs. 1, 2, and 4). However, from the practical standpoint, it can be quite complicated to build a VGT into the bottom of a concrete bridge's span as compared to building it into a pier top. It is also impractical to embed the upper VGT into steel-girder bridge superstructure. This consideration led to the "Single-V Design" (Fig. 5), a subgroup of the innovative V-connector products family.

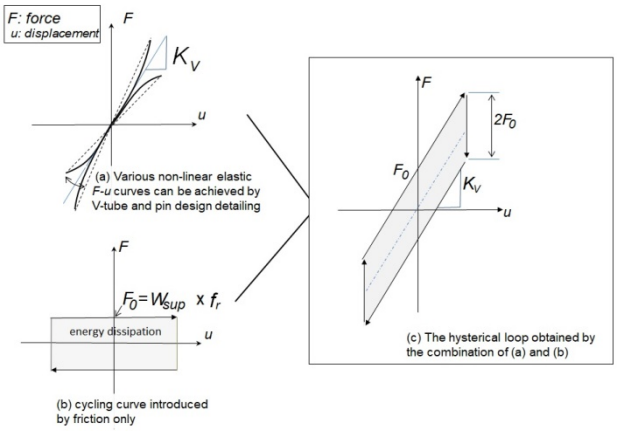

Fig. 3. Hysteresis behavior of the V-connector

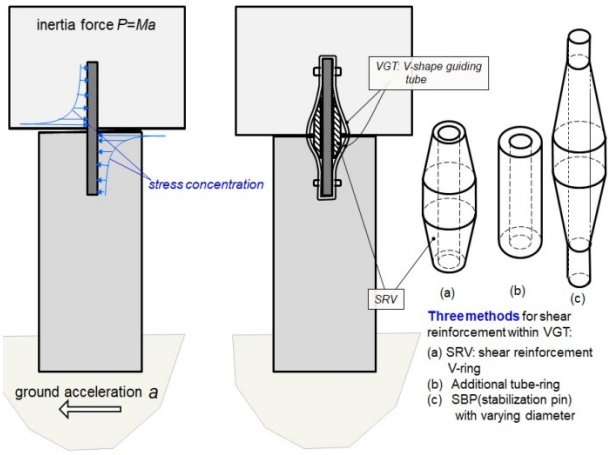

Fig. 4. Innovative design of the pin reinforcement

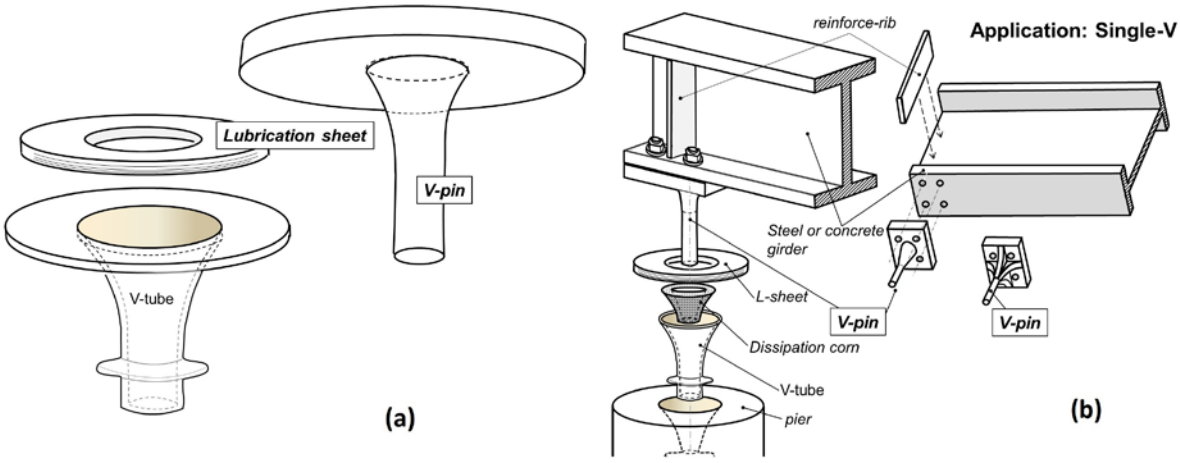

Fig. 5: (a) "Single-V" design of the connector, by which the pin is attached to a pad that is directly mounted to the bottom of a bridge superstructure; (b) Application to a steel-girder bridge.

3. Investigation

After extensive research and design work, two sets of V-connector designs were developed for the two benchmark bridges. The V-connector specimens were then manufactured and tested to prove and validate the introduced innovative concept. The investigation comprised the following four activities:

- Theoretical model development
- Numerical simulation-based parametric studies – design of numerical experiments
- Product design for benchmark bridge application
- Pushover test for proof-of-concept and performance validation

While the VGT geometry enables self-centering which is an advantage of the V-connectors for ABC, this investigation focuses on the seismic isolation function of the V-connectors.

3.1 Theoretical Model

Currently, seismic isolation (Fig.6) has found broad application world-wide. However, by roller bearing, the connection between the superstructure and the pier lacks stability and there is also no capability to restore the system to its original condition after an earthquake. Therefore, the practically-applicable seismic isolation bearings either adopt sliding contact (e.g. over a spherical surface) between two connected parts or rely on the bearing's self-deformation to achieve temporal relative separation similar to that by a roller bearing. An example of the former type is friction pendulum bearing (FP) and that of the latter, elastomeric bearing (EM). While these currently-applied isolation bearings provide much better performance than does a roller bearing shown in Fig. 6, they generally do not provide enhanced structural integrity seen in a CIP structure, which, along with other drawbacks, has limited their applicability. Therefore, a motivation for this research was to develop a connector technology that would enable faster bridge construction without sacrificing the robustness of a CIP bridge.

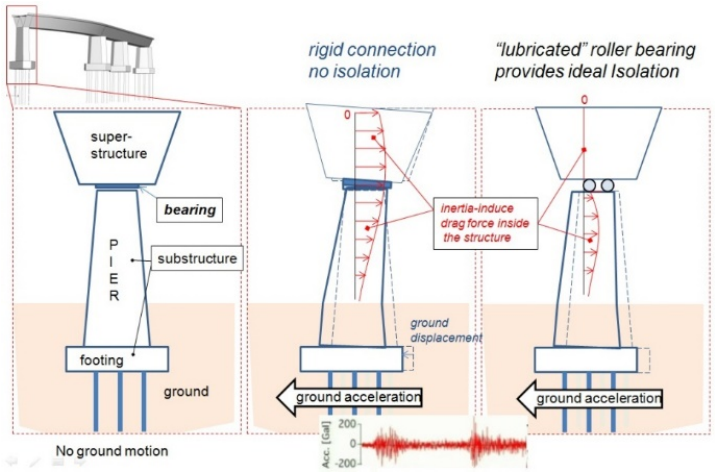

Fig. 6 The concept of "seismic isolation", where the roller bearing (right most) allows relative horizontal motion between the deck and the pier top, confining the ground motion-induced impact to the footing within the substructure.

To this end, the mechanism of how a V-connector (Fig. 2) works in a bridge can be characterized by a simple mechanical model illustrated in Fig. 7(a). The model presumes that the bridge substructure, including the pier and the isolation device, stays in elastic condition. The relationship between P, the earthquake-induced inertia force, and Δ, the corresponding horizontal movement of the superstructure, is represented by the P-Δ curve (Fig. 7c). Since Δ is the sum of Δ_{iso} and Δ_{sub}, the horizontal displacements caused by the isolator and the substructure, respectively, the bearing-pier model (Fig. 7b) is to establish the P-Δ_{iso} curve (Fig. 7c) that indicates whether the structural system has sufficient seismic resistance. This curve deviates from linear elastic behavior when P is greater than Q_d, the static friction resistance, when Δ_{iso}, the nonlinear lateral motion created by the isolation device (such as a V-connector), occurs. If there is no isolation device, i.e. $\Delta_{iso} = 0$, the corresponding P-Δ curve will be linear until the substructure reaches its yield load, i.e. when $P=P_e$ in Fig. 7(c). By contrast, the presence of the isolation device results in the actual force $P=P(\Delta)$ shown in Fig. 7(c). The ratio between Pe and $P(\Delta)$ is termed, the ductile factor, and denoted by R. The ratio between $P(\Delta)$ and $\Delta_{iso} + \Delta_{sub}$, or alternatively, the effective stiffness, denoted as $K_{eff\ in}$ Fig. 7(c), characterizes the seismic performance of a structural system. As Δ_{iso} becomes larger, K_{eff} generally becomes smaller, which leads to better seismic resistance. For displacement-based seismic resistance design using isolators, this research suggests that, for the expected performance, at least the following two conditions are necessary:

C1: a seismic isolator that is able to provide sufficient separation deflection Δ_{iso} to assure that the resulting effective stiffness will be low enough to keep the corresponding force on the substructure below the predesigned allowance; and

C2: an appropriate damping mechanism that effectively dissipates vibration-induced energy and to avoid vibration resonance.

These two conditions are termed performance-based criteria for seismic isolation design.

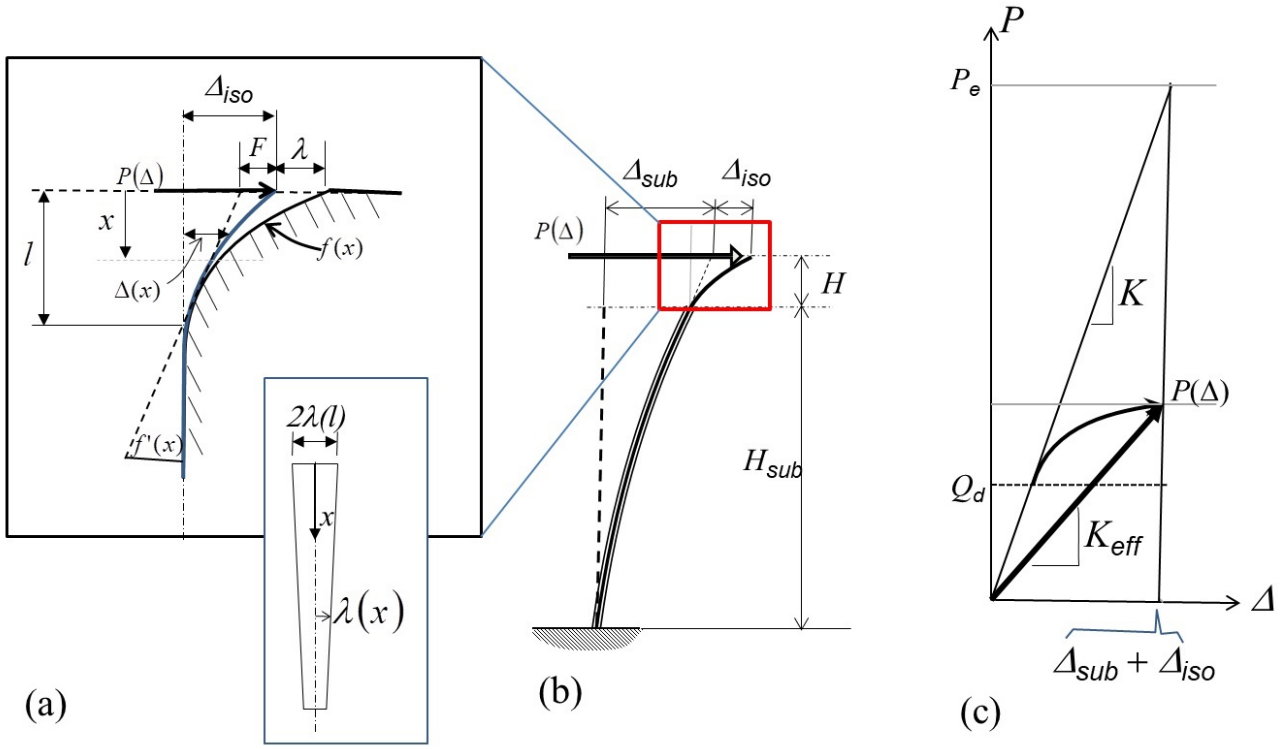

Fig. 7: (a) the model to establish the governing differential equation to determinate the curvature of V-connector, where λ(x) is the function of the radius of the stabilization pin (SBP) shown earlier in Fig. 2, which may be varying along its longitudinal direction denoted by the coordinate *x*; (b) the bearing-pier model, where horizontal deflection Δ is the sum of the part contributed by substructure (Δ_{sub}) and that by the isolation device (Δ_{iso}); (c) characterization of the relationship between earthquake-induced inertia force (*P*), and the corresponding horizontal movement of the superstructure (Δ).

The structural features of V-connector assure that it can be designed to satisfy the above two criteria. However, to achieve best performance, the effect of each relevant parameter needs to be understood so as to obtain optimized design parameters. The parameters to consider include, but not limited to, geometry, size, and material. Among these, the curvature of the V-shaped crater part of the VGT is most crucial. Fig. 7(a) is the model based on the kinetics of the SBP deformation within the crater part of the VGT when the lateral force *P* acts, from which a governing ordinary differential equation was established to quantify the curvature function, *f(x)*, for the crater part:

$$f(x) - \lambda(x) + x\frac{df(x)}{dx} + F\big(P, x, \lambda(x)\big) = \Delta_{ISO} \tag{1}$$

with the following two penalties:

$$\frac{P \cdot x}{E \cdot I(\lambda(x))} \leq \sigma_Y \tag{2}$$

$$\frac{P}{\pi\lambda^2} \leq \tau_Y \tag{3}$$

where $\lambda(x)$ is the radius of the pin that may vary and $I\big(\lambda(x)\big)$ is the pin's sectional bending moment; $F\big(P, x, \lambda(x)\big)$ is its end deflection under the load *P* (see Fig.7); *E*, σ_Y, τ_Y are the pin's Young's modulus and yield and shear strengths, respectively.

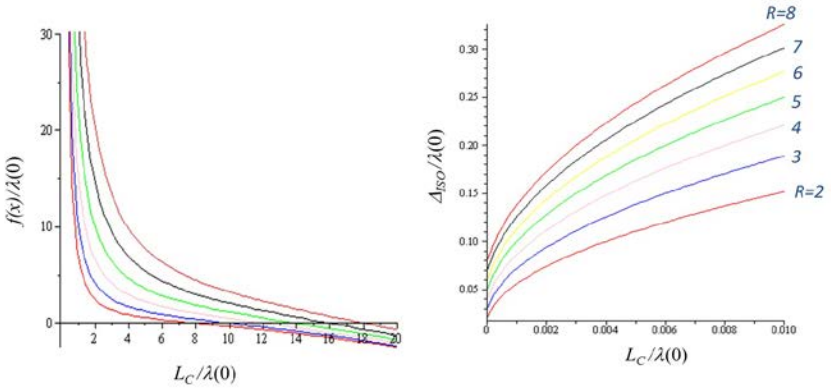

(a) (b)

Fig. 8: (a) A group of solutions for the governing equation (1), which provides the hint for the curvature's design for a VGT; (b) The corresponding relationship between the opening radius of VGT and the V-shaped crater's depth L_C shown in Fig. 2.

For simplification, assuming λ to be constant and the load-deflection relationship approximated by a quadratic polynomial, $a_0\Delta^{0.5} + a_1\Delta$, an analytical solution of Equation (1) above can be obtained. The solutions are plotted in Fig. 8(a). Taking the ductile factor R as the governing parameter, the corresponding relationship between the VGT's opening radius and its depth is shown in Fig. 8(b). The solutions of Equation (1) quantify the relationship between the V-curvature and the pin geometry when the latter is defined. Optimization of the pin geometry will lead to a design with better performance but this will also compromise the uniqueness of the differential equation solution. More sophisticated analysis will be needed to obtain more generalized solutions, which will, however, require significant resources in terms of time and funds. In the present investigation, numerical analysis is utilized to obtain optimized parameters.

3.2 Design of Numerical Experiments (DONE) for Parametric Optimization

This subsection discusses the numerical simulations of the FE models conducted for the V-connectors and the bridges shown earlier in Fig. 1 at two levels -- (i) V-connector detailing, with varying sizes and geometries; and (ii) full-scale bridge models with installed V-connectors in order to investigate their response to seismic events with varying design parameters. The computational results, in conjunction with the analysis of the theoretical model described in the previous section, were analyzed to screen out optimized-parameter connector group. This methodology is termed "Design of Numerical Experiments" (DONE) by the researcher.

3.2.1 Three-Dimensional DONE for V-Connectors

This subsection considers the following two objectives:

(i) Prove that V-connection can provide similar or higher strength to a bridge to enable it to sustain a strong earthquake as compared with conventional pin-cylinder hole connection using the same materials.
(ii) Identify optimized design parameters.

Computational simulations were conducted for a series of 3D FE models of a bridge span-pier connection via embedded pin or V-connectors (Fig. 9). The investigation compared the performance of four types of methods: Ma – a connection using a conventional pin within a cylindrical hole in the concrete matrix; Mb – a straight pin in a cylindrical metal tube inserted into the concrete matrix, i.e. pipe-pin connection; Mc – a V-connector using a straight SBP and a VGT with curvature opening; and Md – a V-connector using SBP with varying diameters in the V-crater part of the VGT. The corresponding simulations included two groups: group I: the FE models of four specimens for each method with the same vertical load, horizontal acceleration, friction coefficient, and materials for the pin, tube, and concrete matrix; as well as the same diameter for the straight pin and for the straight part of the pins with varying parameters; group II: the FE models for the methods Mc and Md with varying diameters of the pins and VGTs. The failure load results for group I are listed in Table I. A FE mesh-network for method Mc is given on the left-most of Fig. 9; another three meshes are the FE models of group II for method Md. Fig. 10 provides the snapshot of computed progressive stress distribution with increasing load for the FE model on the second from left in Fig. 9, which is an example of method Md and shows that the high peak stress has

been redistributed over a relatively large area with lower peak value when the applied load increases. Fig.11 is a comparison of the failure patterns among the methods Mb, Mc, and Md, from left to right. It is notable that, for the failure pattern of Mb (Fig. 11, left-most), the localized shear stress cuts the pin inserted into the cylindrical hole without proximity. By contrasts, for the failure patterns of Mc and Md (Fig. 11, middle and right-most), when lateral deformation becomes large, the SBP bends to the wall of the crater-part of the VGT, which transfers shear stress localization into compression distributed over the circumferential surface of the SBP, which explains the difference in the levels of failure loads given in Table I.

These 3D results indicate no remarkable difference in local mechanical behavior, including local deformation and stress distribution, between the upper and lower VGTs as well as the two end-parts of the pin. In other words, the V-connector is mechanically locally symmetric to the contact surface of the two connected parts. Therefore, the upper and lower VGTs can be designed with the same geometries where each provides half of the horizontal deformation tolerance.

Table I: Comparison of the Load Capacity of Four Connection Methods

	Method Ma	Method Mb	Method Mc	Method Md
$F_{failure}/F_{failure}^{Ma}$	1	1.032	1.154	1.61

$F_{failure}^{Ma}$: The failure load of method Ma.

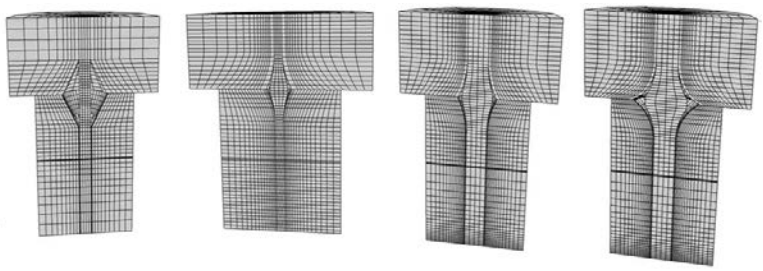

Fig. 9: FE models of the V-connectors with various design parameters.

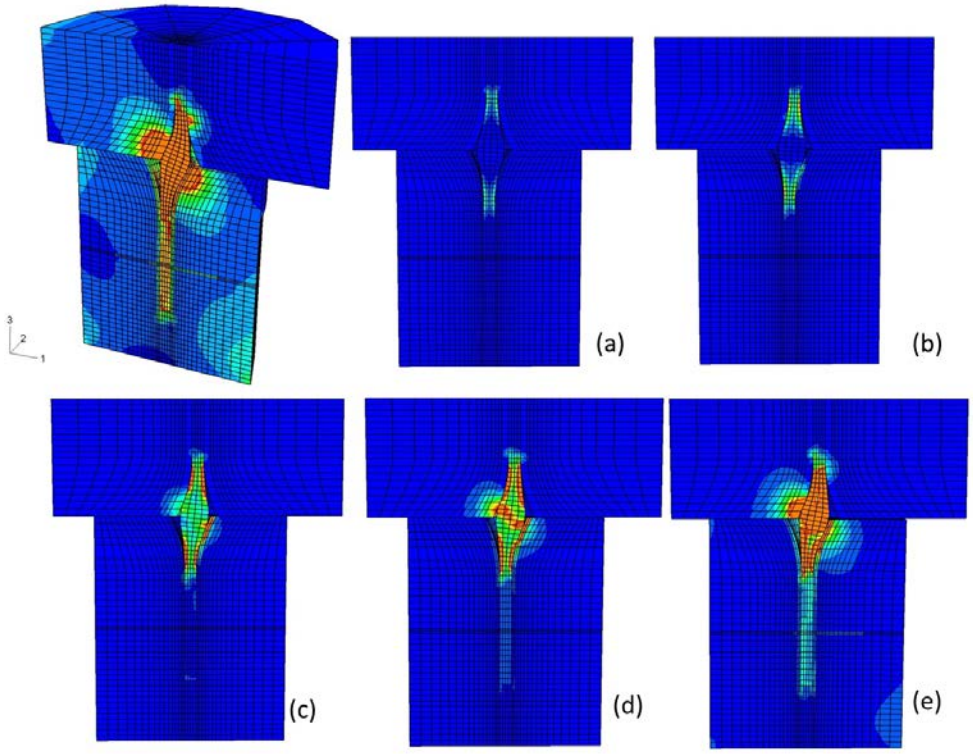

Fig. 10: A computation example: the relatively-high stress first occurs in the two ends of the pin that are inserted into the cylindrical tube; then the high stress area progressively moves to the middle part of the pin with shear force increase. The computation methods are introduced in [16-20] and also in [10-12].

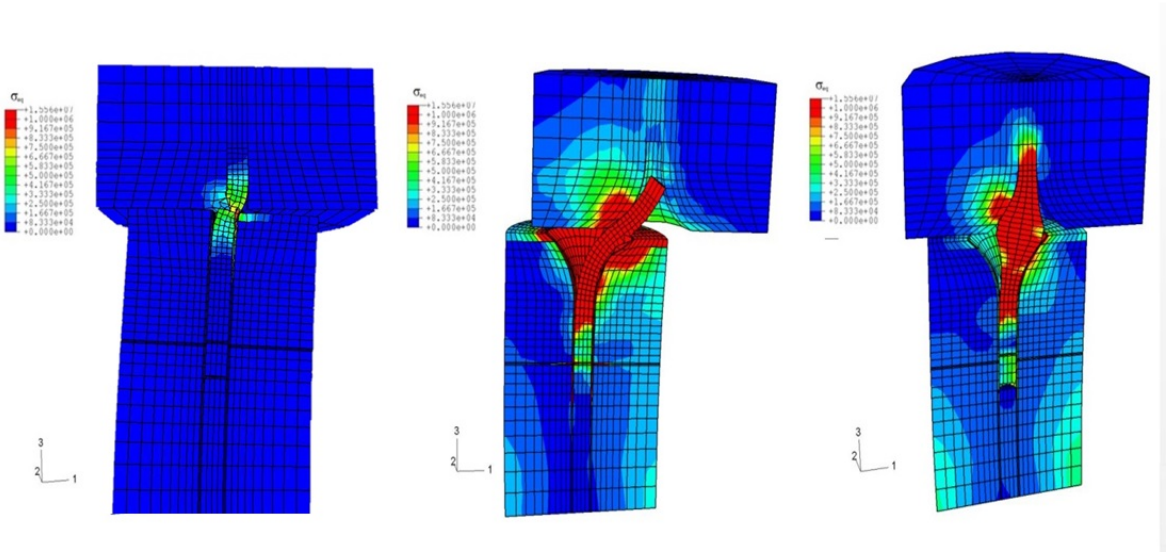

Fig. 11. Failure patterns, from left to right corresponding to methods Mb, Mc, and Md, respectively, in group I simulation; for the pattern of method Mb on the left with the connection by pin-in-cylindrical holes, high stress concentration occurred in a localized area. The failure loads for the four connection methods with reference to Method Ma are given in Table I.

All FE computations demonstrated that the V-connector produced hysteresis cyclic loops as predicted by the plot on the left in Fig.3. This prediction was also verified by experimental results to be discussed later. The hysteresis loop, when the deformation of the connected substructure has been counted, can be plotted as that shown in Fig. 12a, where the enclosed dark area represents the energy dissipated during each vibration cycle. The vibration energy is transferred into heat. This mechanism is the key for a V-connector to be a seismic isolator. If there is no such energy dissipation, earthquake-induced vibration will cause the connected structure system to vibrate with increased amplitude because of accumulated vibration energy (resonating vibration) that will eventually destroy the structure. According to the AASHTO bridge specifications for seismic design [8], for a single isolator and substructure, an equivalent damping ratio ξ is defined as follows:

$$\xi = \frac{Energy\ Dissipated\ (the\ hysterical\ loop\ enclosed\ area)}{2\pi K_{eff}(\Delta_{total})^2} \tag{4}$$

where the definitions of K_{eff} and Δ_{total} are provided in Fig. 12a.

For simplification in this report, the contribution of the substructure is omitted. So, according to Figs. 2, 3, and 12a as well as the associated analysis, the equivalent damping ratio ξ for a V-connector can be approximated by the following expression:

$$\xi = \frac{f_r \cdot W_{sup}}{\pi K_{eff}\Delta_{total}} \tag{5}$$

where W_{sup} is the weight of the superstructure carried by the isolator; f_r is the friction coefficient (see Fig. 12a).

Based on the computational results, in conjunction with the theoretical analysis in the previous subsection, the plots in Fig. 12b provide hints for the V-connector's design parameters shown on the left in the figure.

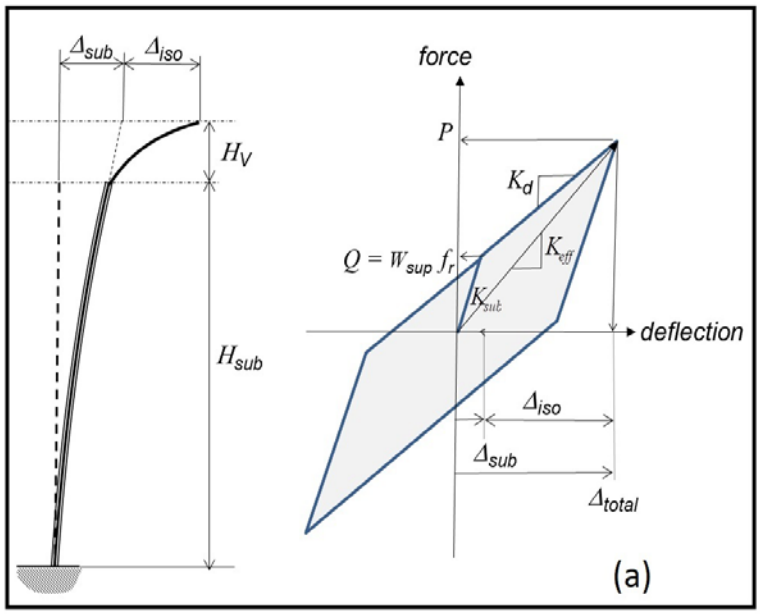

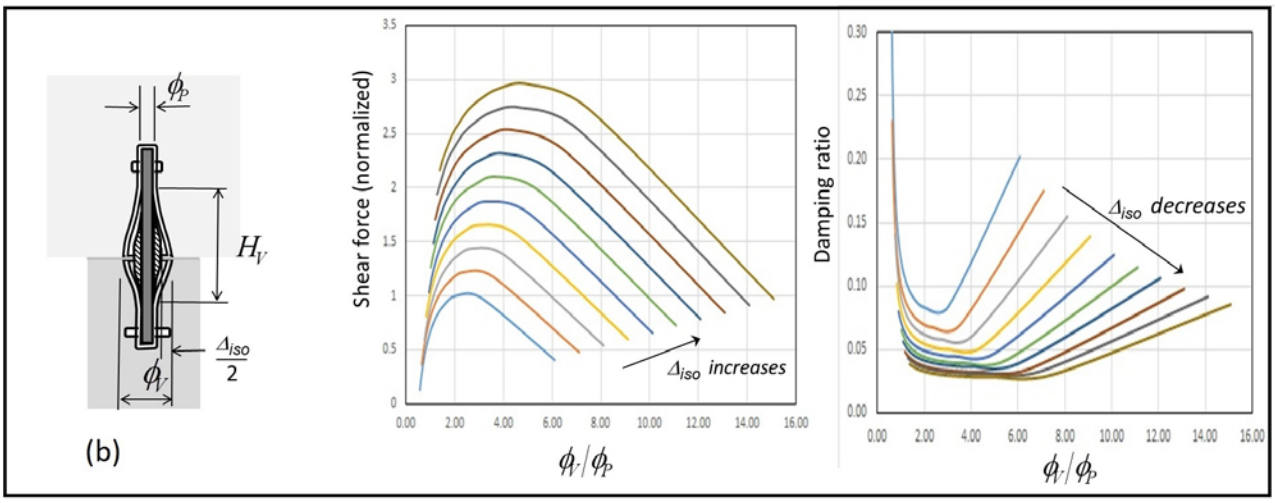

Fig. 12 (a) Hysteresis loop (right) for the structural system (left) which is a pier of height H_{sub} with a V-connector above, deformed due to carried superstructure, [see 6-8, 21]; (b) The semi-empirical guidance illustrated in the diagrams in the middle and right for the design parameters denoted in the plot of the V-connector on left.

3.2.2 Benchmark Bridges

This subsection determines the requirements of the benchmark bridges in order to identify the load parameters of the V-connectors for these bridges and to manufacture those connectors for experimental verification and validation.

3.2.2.1 The AASHTO Benchmark Bridge (Fig. 1a)

Key parameters of the 3-span benchmark highway bridge are listed in Table II below. More detailed information on the bridges is provided in [8]. The focus of this investigation was to design V-connectors for the bearing on the pier under the vertical load of 219 kips and the abutment under the vertical load of 168 kips.

Table II: Key Parameters of the 3-Span Bridge

Support	Number of Girders/Bearings per Support	Weight of Superstructure at Each Bearing (kips)	Participating Weight of Each Pier (kips)	Effective Weight on Each Support (kips)	Stiffness of Each Pier in Both Directions (kip/in)	Minimum Column Shear Strength (kips)
Abutment 1	3	168		168		

Pier 1	3	219	128.13	785.31	289	128
Pier 2	3	219	128.13	785.31	289	128
Abutment 2	3	168		168		

3.2.2.2 The Railway Bridge (Fig. 1b)

The non-skew three-span railroad bridge has the span length of 105 feet but two combinations of pier pairs with respect to height – piers each 33 feet high and pier pairs 33 and 50 feet high. Also, two types of superstructures – a simply-supported precast concrete box-girder, for example, three individual girders over each span (Fig. 13) and another single continuous orthotropic box-girder over three spans (Fig. 14) – were analyzed. As illustrated in the bottom part of Fig. 13, precast concrete box-girder with varying cross section areas were designed to smooth out the concentrated stress due to the bearing support at the beam's ends. For each case, the top cross-section geometries of the piers are given in Fig. 15. These bridges, designed for rail transportation, generally have high live-load induced lateral turnover moments.

Following AASHTO LRFD 5.10.11.14.1c, the maximum cross section dimensions at the pier top ends (Fig. 15) were chosen for the extension reinforcement. With this extension, it is assumed that the cross section areas of all piers are reduced to half while their outer perimeters remain unchanged, i.e. each pier has the internal cavity with the wall thickness of 2.1feet for both cases in Fig. 15.

An equal length span design may not be appropriate for a three-span continuous bridge (Fig. 14), which is however just an example to evaluate the functions of the V-connectors.

The superstructure weight, including permanent loads, averages 16.15 *klf* (kips/ft) for the concrete girder in Fig. 13, with the total weight of 1695 *kips* per span. It is 6.85 *klf* for the orthotropic box-girder in Fig. 15, with the total weight of 719.3 *kips* per span and *2160* kips for the three spans. For the continuous span bridge, the unfactored dead load carried by each abutment is 288 *kips* and that by each pier 791.5 *kips*. The mass of the product of the end cross section area times one third the clear pier height is chosen to calculate the maximum shear[1]. The cross-sectional area is 238.54 ft^2 for the pier top of the simply-supported span, i.e. 35.8 *klf* for extension and 17.9 *klf* for the regular part. For the continuous span, the cross-sectional area is 146.26 ft^2 i.e. 21.9 *klf* for extension and 10.97 *klf* for the regular part. For both cases, rebar reinforcement takes 2.5% of the total cross-sectional area. Material properties and bearings' loading conditions are given in Tables III to V.

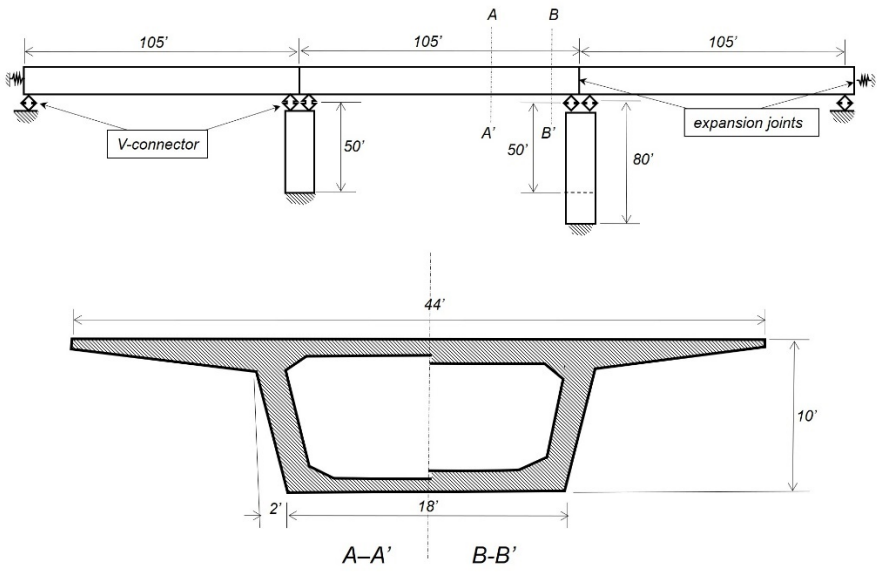

Fig. 13: Benchmark railroad bridge I: three-span simply-supported precast concrete box-girder bridge. To reduce the stress peak in areas around bearings locations, thicker box wall has been designed at B-B section, although the bending moment here is lower than section A-A.

[1] LRFD 5.10 requires the mass of half height of substructure for the shear force calculation.

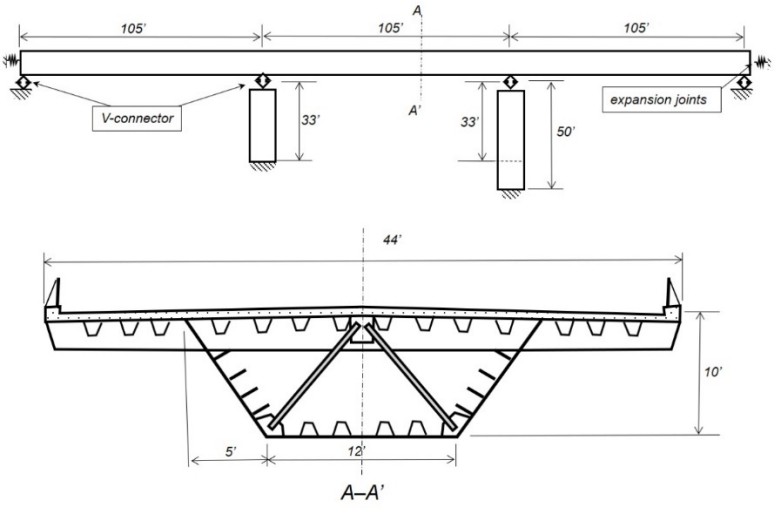

Fig. 14: Benchmark railroad bridge II: three-span continuous orthotropic box-girder bridge

n

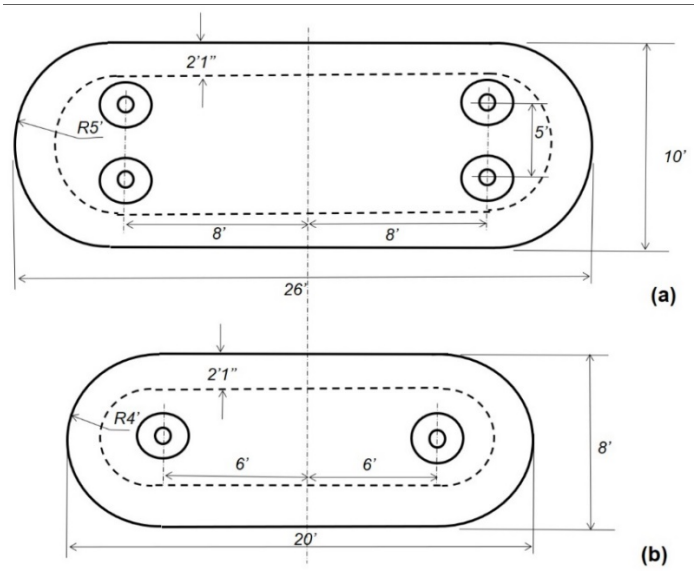

Fig. 15: Top cross-section geometries of the piers: (a) for simply-supported concrete box-girder, where 4 V-connectors are located for the two end parts of the two adjacent girders; (b) for continuous orthotropic box-girder, where only 2 V-connectors are located because of the carried continuous girder.

Table III: Material Properties for the Bridges (Figs. 13 and 14).

Concrete Box-Girder Bridge (Fig. 13)								Orthotropic Box-Girder Bridge ASTM A709-Grade 50 (Fig. 14)			
Concrete				2.5% Rebar (ASTM A709-grade36)							
f_c'	$f_{rapture}$	E_c	ρ_c	σ_Y	σ_u	E_s	ρ_s	σ_Y	σ_u	E_s	ρ_s
4 *ksi*	0.475 *ksi*	4000 *Ksi*	150 *pcf*	36 *ksi*	58 *ksi*	29000 *ksi*	487 *Pcf*	50 *ksi*	65 *ksi*	29000 *ksi*	487 *pcf*

Table IV: Moment of Inertia at the Weakest Cross-Sections for the Flexural and Column Members

	Moment of Inertia and *EI*	Concrete Girder	Pier for Concrete Girder	Orthotropic Steel Girder	Pier for Steel Girder
Strong Direction	I (in^4)	207.3x10^6	151.1x10^6	17.7x10^6	53.9x10^6
	EI (kips-in^2)	829.2x10^9	604.4.9x10^9	513.3x10^9	215.6x10^9
Weak Direction	I (in^4)	25.5x10^6	22.9x10^6	3.2x10^6	9.73x10^6
	EI (kips-in^2)	***102. x10^9***	91.6x10^9	***92.8x10^9***	38.9 x10^9

Table V: Weight per Span and the Weight Carried by Each Bearing

	Line-Weight of Span (klf)	Total weight (kips)	Weight per Bearing on Pier Top (kips)	Weight per Bearing on Abutment (kips)
Concrete Girder Bridge	16.15	1695x3	424	424
Continuous Orthotropic Bridge	6.85	2160	198	144

Benchmark bridges (Figs. 13 and 14) at four sites, representing three of the four seismic zones according to AASHTO LRFD [7-9], were investigated. The corresponding parameters are given in Table VI.

Table VI. Investigated Sites

Site No.	Zones	Site Class	PGA (g)	S_s (g)	S_1 (g)	A_s (g)	S_{DS} (g)	S_{D1} (g)	Operation Category	System adjustment factor
1	I	D	0.039	0.085	0.034	0.0624	0.136	0.0816	Essential	0.75
2	III	C	0.403	0.886	0.301	0.403	0.926	0.452	Other	0.66
3	IV	C	0.476	1.122	0.406	0.476	1.122	0.566	Essential	0.75
4	IV	B	1.067	1.915	0.561	1.067	1.915	0.561	Critical	1

where the operation category is defined according to section 3.10.7.1 in the AASHTO LRFD Code [7] and the system adjustment factors are defined according to Section 8.22 of the AASHTO Isolation Design Code [8]

Geotechnical properties of a specific location as well as its liquefaction potential may significantly reduce a bridge pier's stiffness and result in a rather large pier top displacement, as indicated by the model in Fig. 16. To consider the foundation's contribution to substructure stiffness, Table VII provides estimates of the depth of the maximum bending moment, d_m, and the equivalent depth of deflection, d_t, for the six site classifications in the AASHTO Design Code. The d_m and d_t for the three sites, B, C, and D are applied to the cases listed in Table VI.

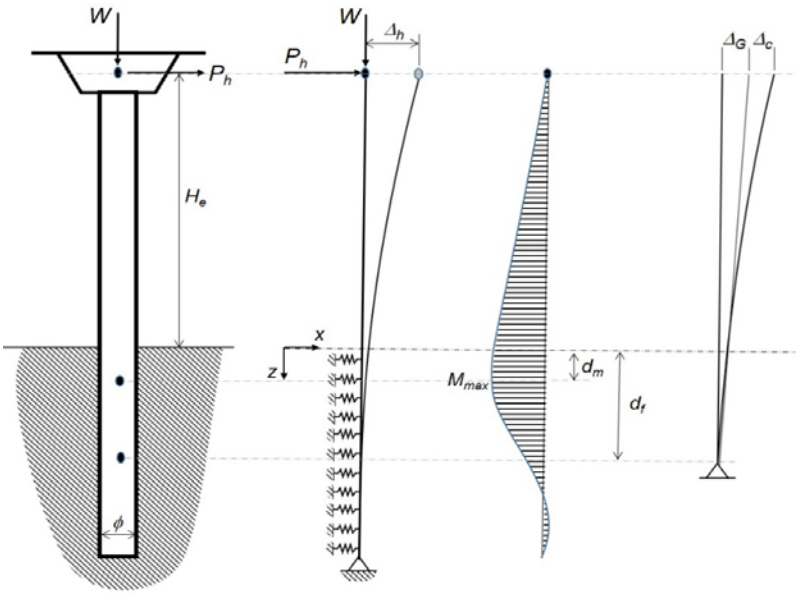

Fig. 16. Model considering soil-substructure interaction [6,-8], [21,23-26]

Table VII: The Maximum Bending Moment d_m and Equivalent Depth of Deflection d_t for the Six Site Classifications in the AASHTO Design Code

	Site A	Site B	Site C	Site D	Site E	Site F
d_m	0	0.3 ϕ	0.7 ϕ	1.2 ϕ	1.8 ϕ	2.5 ϕ
d_t	0	0.8 ϕ	1.7 ϕ	2.7 ϕ	3.8 ϕ	5 ϕ

where ϕ is the maximum transverse dimension facing the bending direction

3.2.2.3 Numerical Models

To consider global responses, Fig. 17a shows a beam FE model for design calculations of the bridges in Figs. 13 and 14. The 3D FE models were established to investigate the effects of local detailing, for which Fig. 17b provides an example.

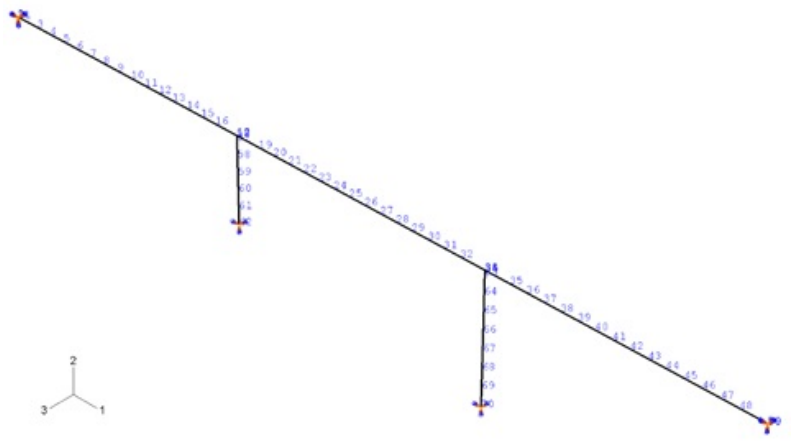

Fig. 17a: Beam model to analyze global effects such as natural frequencies and forces distributions; the computation methods are introduced in [7, 16-20, 23-26], also in [10-12].

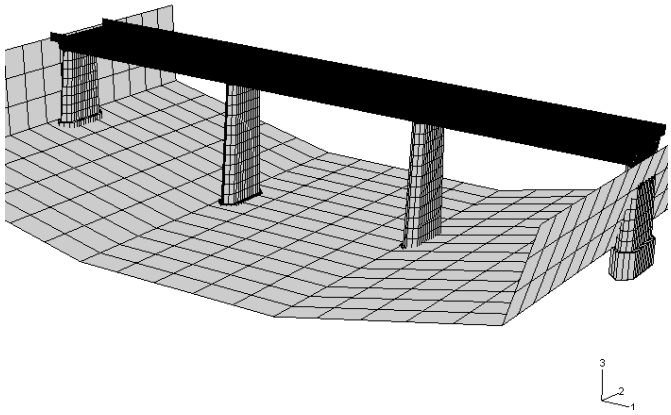

Fig. 17b: 3D FE model to analyze the effects of detailing; the computation methods are introduced in [16-20, 21, 23-26], also in [10-12].

3.2.2.4 Results of Numerical Analysis – Natural Frequencies

Based on AASHTO's multimode elastic method, the first 20 orders of natural frequencies and the corresponding vibration modes were investigated for the bridges in Figs. 13 and 14. For each bridge, there are three natural frequencies that dominate the deformation patterns along three orthogonal directions in the 3D space; these deformation patterns were chosen for design analysis. Two classes of models were analyzed. The first class comprised bridge models with high stiffness connection joints (similar to rock-bearing) between the super- and substructures; the corresponding three natural frequencies are the lowest order eigenfrequencies along each direction that satisfy the following criteria:

$$\frac{Model\ Effective\ Mass}{Model\ Total\ Mass} \geq 5\% \qquad \text{and} \qquad |model\ participation\ factor| \geq 0.1 \tag{6}$$

For comparison, the second class of bridge models was with V-connections. For the analysis of this class of models, the lowest natural frequencies were selected for the same deformation patterns as those in the corresponding model in the first class. Shown in Fig. 18 are the computed deformation patterns. Table VIII lists the corresponding natural frequencies by presuming the ductile factor R to be 3 for the applied V-connector. Fig. 19 is the result for a full-scale 3D bridge with the V-connector, showing the stress contours during dynamic cycling loading.

Table VIII: The First Three Orders of Natural Frequencies of the Benchmark Bridges in Figs. 13 and 14

Type of Structure	Height of Pier (ft)		Connection Joint Classes (I: Rock-Bearing, II: V-Connection)	The Lowest Natural Frequencies along Three Major Directions Satisfying Criteria [6]; (cycle/sec.)		
	Pier 1	Pier 2		Transverse	Longitude	Vertical
Concrete Superstructure (Fig. 13)	50	50	I	1.568	21.75	12.24
			II	0.527	8.168	6.97
	50	80	I	1.5778	23.14	11.351
			II	0.382	6.92	4.773
Steel Superstructure (Fig. 14)	50	50	I	1.359	17.08	9.39
			II	0.714	12.61	8.65

(a) Even pier heights (b) uneven heights of piers

Fig. 18 Vibration patterns for the lowest natural frequencies along three orthogonal directions where the right ones are with V-connectors. This, in conjunction with Table IV, shows that the V-connectors contribute to deformation while reducing frequencies, see also [10-12, 16-20, 23-26].

,

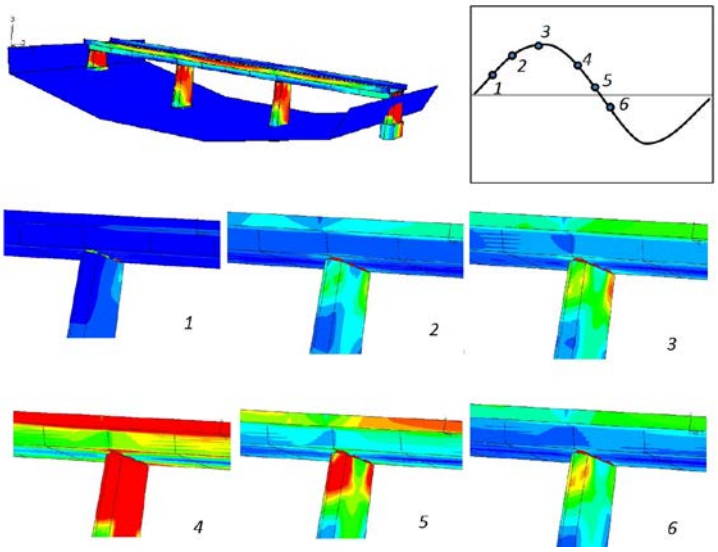

Fig. 19 3D FE analysis to examine the stress distributions around the beam-pier joints with V-connectors when the bridge model in Fig. 17(b) is under load cycles. These computational plots show discontinuity in stress contours around the joint area, verifying the isolation function of the connector.
The computation methods are introduced in [16-20] and also in [10-12].

In practice, it is not always convenient to embed an upper VGT into the bottom of a concrete bridge beam. In [4-6], a Single-V design was developed (Fig. 5), which included two design subgroups of the V-connector family -- fixed-end pin design and hinge-end pin (HP) design -- shown on the rightmost in Fig. 20. For both, the top part is directly mounted onto the bottom surface of a bridge beam, which is similar to a conventional bearing pad.

As stated previously, there is no substantial difference from the perspectives of local mechanical behavior between the upper and lower VGTs; each provides half of the horizontal deformation tolerance for vibration isolation. This implies that the Single-V HP design, shown in Fig. 20, has an isolation capacity of 50% of that of the double-V design (Fig. 2), if the tube parameters are the same. Since the upper part of a V-connector with HP design can be mounted onto the bottom of a bridge beam like a conventional bearing, it has practical advantages. Therefore, two groups of V-connector specimens with HP were designed and manufactured for cases presented in Table IX.

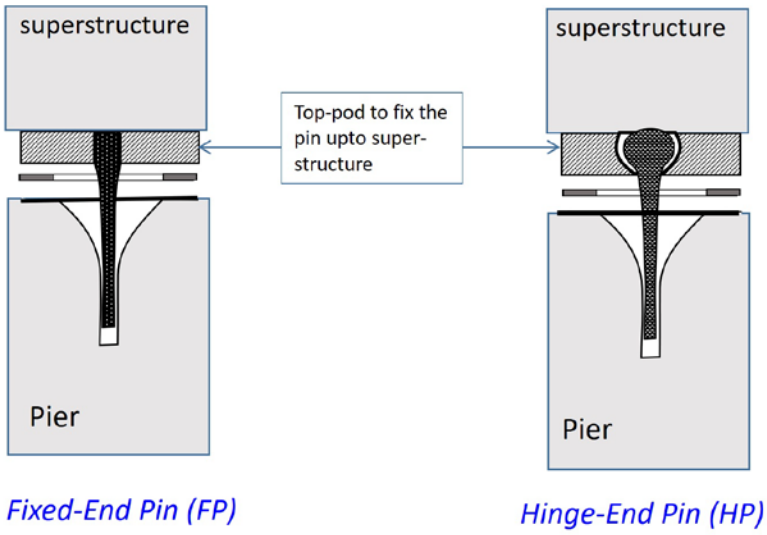

Fig. 20: Two subgroup designs of the V-connector product family

3.3 Requirement to Accommodate Out-of-Plane Rotation [7-9,34]

Bridge bearings are generally required to have a capacity to accommodate a span beam's end rotation, particularly when the rotation takes place out of the horizontal plane (Fig. 21a and Table IX). In practice, such rotation can be caused by live load, thermal expansion, or erection tolerance. Spherical contact surface is a conventional method for this purpose in the bearing design. However, when significant horizontal displacement occurs at a long-span beam's end (often caused by thermal expansion/shrinkage or a strong earthquake), the contact of spherical surfaces will change into a line-like contact, which may result in localized surface damage (Fig. 21b). Therefore, the V-connector utilizes a specially designed washer for this purpose.

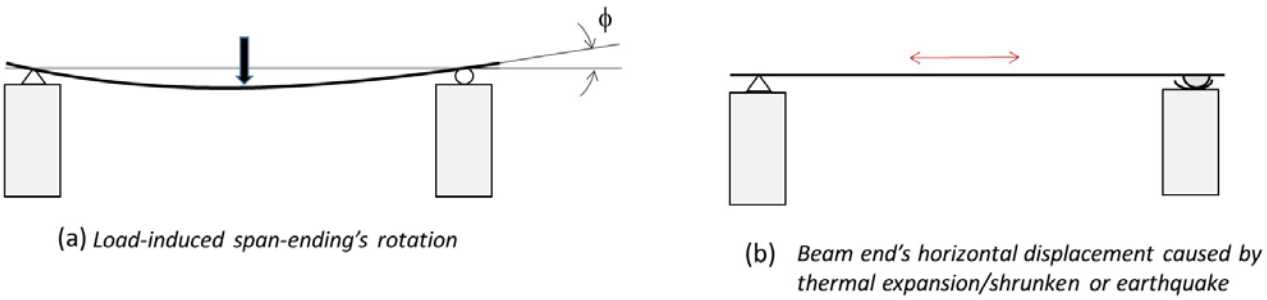

Fig. 21 Requirement of bridge bearing to accommodate out-of-plane rotation

Table IX: Required Tolerance for Bridge Ending Rotation (rad)

Road & Highway Bridges	Railway Bridges										
	Speed Lower than 200km/hr					High-Speed Rail					
US [1]	US [2]	Germany [3]						P.R.China [3]			
		Single Track		Double Tracks				Ballasted Track		Ballastless Track	
		E	P	E	P	E	P	E	P	E	P
0.005	0.01+	0.0065	0.01	0.0035	0.005	0.002	0.004	0.002	0.004	0.001	0.002

E: for span-ending bearing above abutment; P: for bearing on pier top.

3.4 Specimen Design and Manufacture and Test Facilities

Based on the analysis described in section 3.2, two groups of V-connectors with HP design (Fig. 20) were manufactured and tested at the PEER Center Laboratory of the University California at Berkeley and the Fengzhe Laboratory in China. The first group of specimens, tested at the PEER Center, is labeled as VC1 group and the second group as VC2 (Table X). Fig. 22 is the CAD assembly drawing for VC2 specimens. Although the two groups have similar geometries, they differ in size as seen in Table X, where the parameters of VC1 are for the AASHTO Bridge (Fig. 1a) and those of VC2 for the rail bridge (Fig 1b). The selection of the pin material is based on (i) strength, (ii) adequate fracture toughness, (iii) corrosion resistance, and (iv) cost-effectiveness. The metal parts of VC1 were manufactured by R. J. Watson Inc., located in Alden, New York, and delivered to the PEER Center Laboratory (Fig. 23a). For VC2 specimens, the VGT was machined from a piece of cast iron, which, together with concrete, was cast into a steel box (Fig. 23b) in the Fengzhe Engineering Development Company, Ltd.

Table X: The Major Differences between VC1 and VC2

	Manufacturing Method of VGT	Pin Material	V-Crater Depth L_C (mm)	Pin Diameter (mm)	Washer	
					Thickness (mm)	Surface Treatment
VC1	Rolling, Welding	ASTM A572 GR50	286	40	20	No
VC2	Machinery, Cast	40Cr (Similar to ASME 5140) without Tempering	310	37	7	Yes

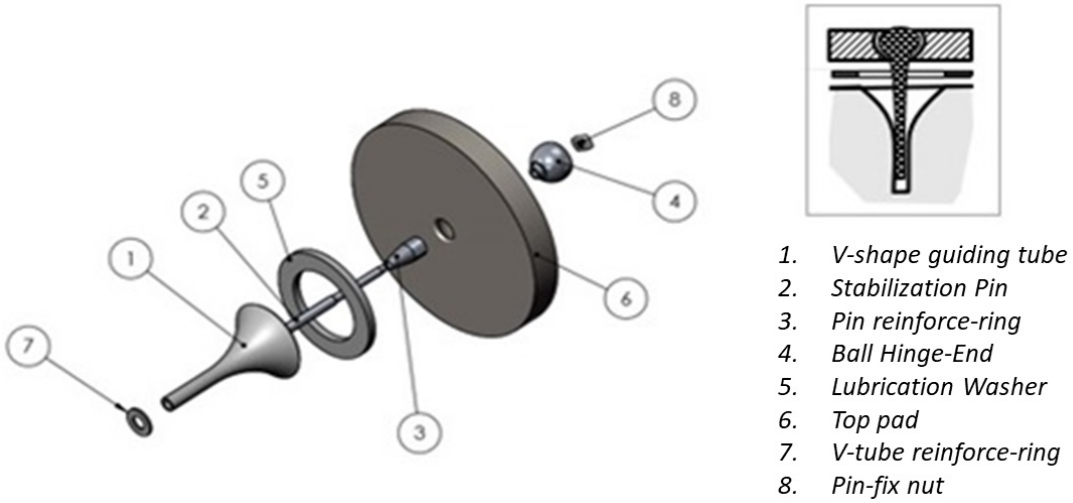

Fig. 22: CAD assembly for the basic design drawing of a HP V-connector's metal parts

For testing VC1 specimens at the PEER Center Laboratory, two concrete elements representing pier and superstructure were cast into two blocks as shown by the diagram on the left-most of Fig. 24. The forces imposed onto the lower concrete block, representing a pier, can be categorized into two classes: (1) the compression imposed on the top-plate above the VGT; and (2) the shear and compression in the concrete block. For the former, the force flow can be approximated by a model like strut-and-tie (Fig. 24, left), which results in the rebar network around the VGT as shown on the right in Fig. 24. For the latter, the rebar network was designed according to the analysis in [35] and is plotted in the upper-left of Fig. 25. The two sets of rebar networks formed the network on the right of Fig. 25 and cast into the lower block of the concrete matrix as shown in Fig. 26. For both specimen groups, polytetrafluoroethylene (PTFE) was used for the washer material but with different thicknesses and surface treatments.

(a) (b)

Fig. 23. VC1 group of V-connectors delivered to PEER Center (left) and VC2 group to the Fengzhe Laboratory in China (right).

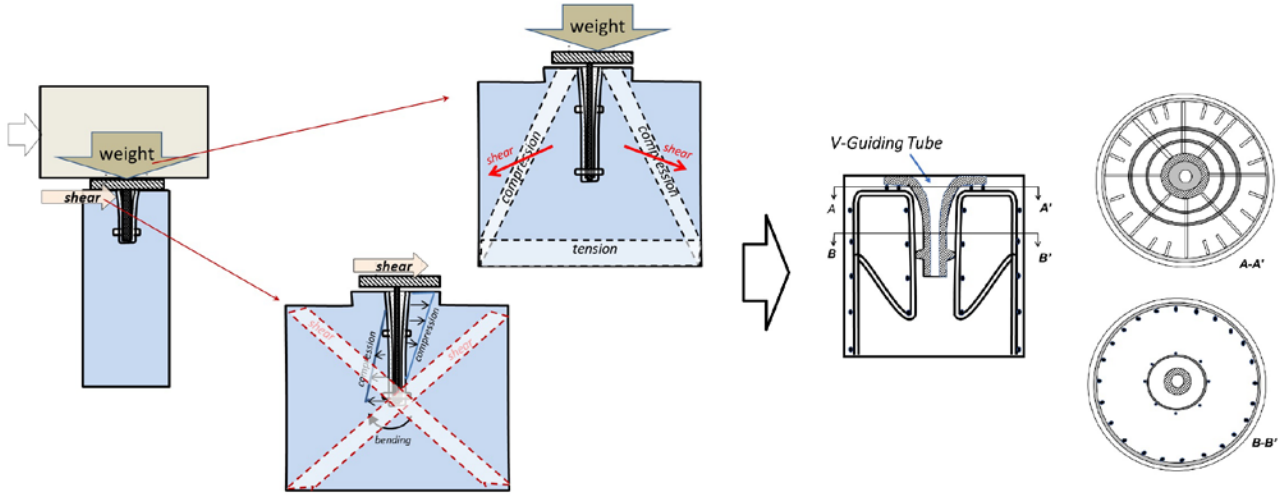

Fig. 24. On the left is a strut and tie-like model to analyze major force flow in the bottom concrete block. On the right is the corresponding arrangement of the local rebar layout surrounding the VGT.

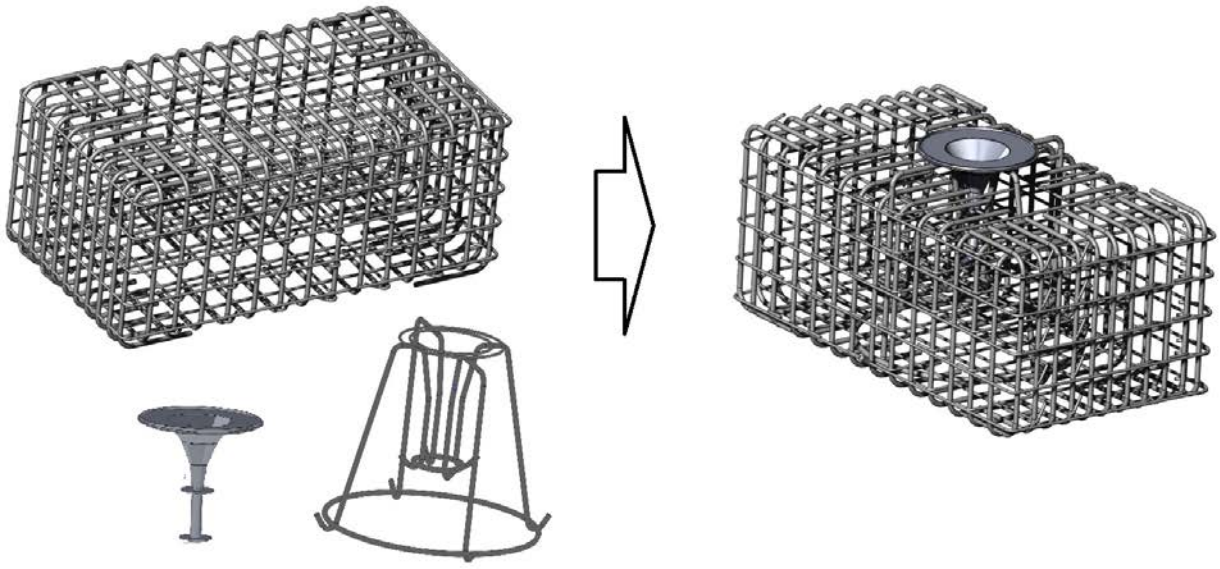

Fig. 25. Left: VGT, the rebar network for the tube locally and the concrete block, designed to reinforce pier to resist earthquake-induced forces [35]. Right: the finished rebar-layout with a V-tube.

Fig. 26. Specimen assembly with two concrete blocks connected by V-connector of the VC1 group at the PEER Center test facility. The photo on the top right corner is a view by Terrestrial Laser Scanner that provides the displacement field of the entire system [13].

Fig. 26 is the photo of test facility at the PEER Center, further elaborated in Fig. 27. The facility includes a beam above the top concrete block to represent a superstructure. The two ends of the beam are connected to two force-actuators (A and B) hinged onto ground to introduce the pull-down force of the same magnitude as the actual weight carried by a bearing for a superstructure of the bridge in Fig. 1. Another two actuators, laid horizontally with one end hinged onto the stable frame and the other end to the top block of the specimen, provide horizontal force to simulate the horizontal inertia caused by the earthquake. Adjusting the difference in displacement between the actuator A and B introduces tilted angle of the top beam and, as a result, the pair of contacted surfaces are no longer parallel to each other, which is similar to the case explained in Fig. 21(a). When the two vertical actuators pull down in a synchronized manner, it simulates the case of no tilt at the bearing.

The facility also includes ten wired sensor channels to collect the displacements at any given point and the data of embedded strain gauges attached to rebar network shown in Fig. 25. A Terrestrial Laser Scanner provides detailed displacement field of the entire system as seen in the image inserted on the upper -right corner of Fig. 26.

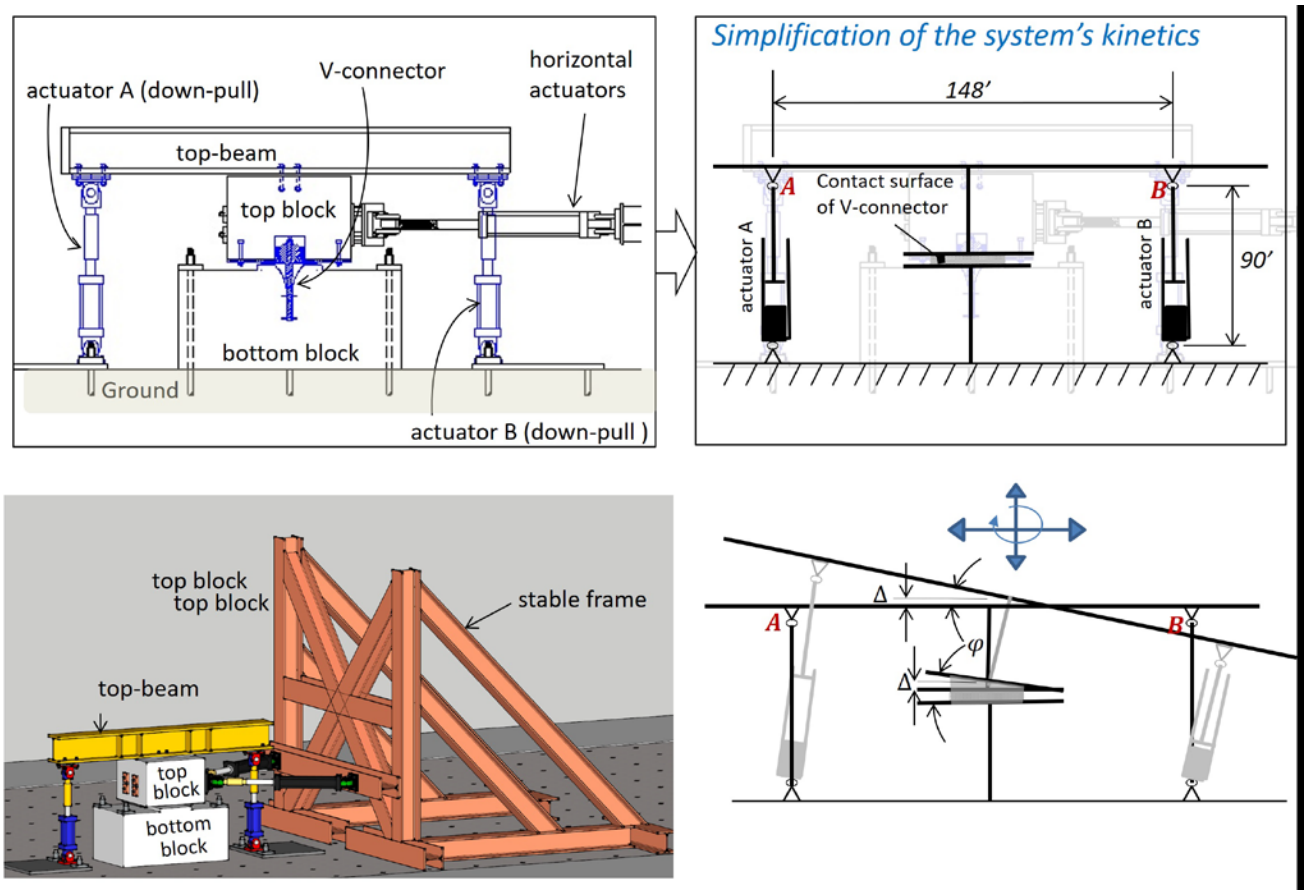

Fig. 27. The kinetics of the PEER Center test facility as illustrated by the sketch on the bottom right. The facility is able to produce motion along any direction within the plane where horizontal force imposed and rotation along the axis perpendicular to the plane.

The photo on the right in Fig. 28 is the machine for testing the VC2 specimens at the Fengzhe Laboratory while the diagram on the left in the figure illustrates how it works. The top block that represents a superstructure has no horizontal motion but is under an imposed compression force that equals to the portion of the superstructure's weight per bearing of the bridge in Fig. 1(a) whereas the bottom block that represents a pier is placed on a guiding rail and pushed back and forth horizontally by the parallel cylindrical actuators to simulate the motion of the superstructure under an earthquake. The relationship of force-displacement is recorded by the test machine.

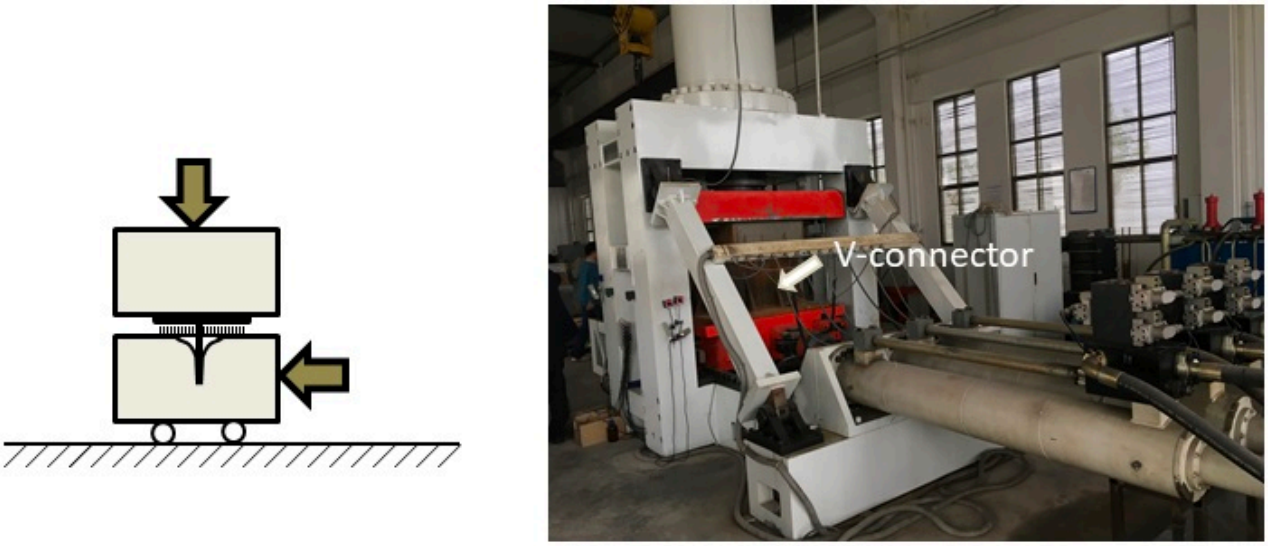

Fig. 28. The compression-shear test machine at the Fengzhe Laboratory, which is able to produce 10000kN (2248kips) compressive force along vertical and horizontal directions simultaneously.

3.5 Test Procedures

For verification and validation of the applicability of the V-connector family to bridge structures, a series of quasi-static pushover tests were conducted that focused on:

(i) verification and validation for seismic isolation capability
(ii) applicability to benchmark bridges
(iii) safety evaluation

The effect of rotation on VC1 group of specimens was investigated using the test facility set-up shown in Fig.27. The safety of the V-connector was evaluated by pushing applied load exceeding the designed capacity in VC2 specimen tests. The loading conditions of the two groups of specimens and test procedures are given in Table XI.

The VC1 specimens were tested following the protocol of the FEMA quasi-static cycling test [13, 14]. The pushover tests were conducted using the facilities at the PEER Center and the Fengzhe Laboratory in China. However, the experiments at the Fengzhe Laboratory were done at four vertical load levels but with only 5 time-steps at each level. Table XI shows the test procedures for the two groups of V-connectors.

Table XI: Test Procedures

Specimen Group	Vertical Load (kips)	Number of Steps	Cycles per Step	Targeted Maximum Deformation (in.)	Deformation Capacity (in.)
VC1	200	10	2	3.9	4
	Following the Quasi-Static Test Protocol of FEMA 461				
VC2	45	3	3	3.5	4
	112	5	3	3.5	
	225	6	5	4.05	

3.6 Results and Analysis

3.6.1 The Isolation Function

Plotted in Fig. 29 are the load vs. deflection curves measured from the tests of both groups of V-connector specimens. These results appear to verify the anticipated hysteresis behavior as predicted in Fig.3 and can also be taken to validate the applicability of the V-connector as a seismic isolator. The initial friction coefficient of VC1 is found to be about 0.055 and the corresponding Q_d (termed, characteristic strength) about 11ksi. However, the friction coefficient does not stay constant and increases to 0.1 when the imposed isolation displacement reaches the target value of 3.9 inches. For VC2, the friction coefficient also varies similarly but decreases from 0.08 to about 0.035 when the imposed vertical load increases from 200kN to 1000kN. These results indicate that surface treatment, loading system set-up, and rotation contribute to the tribological behavior of the system. Nevertheless, the measured friction coefficient is still within the acceptable range. According to the literature, the friction coefficient of PTFE is generally in the 0.03-0.15 range [2]. Although differing in detail, results from the two laboratories do prove the intrinsic dissipation mechanism (predicted in Fig. 3) and demonstrate the repeatability of the seismic isolation capability of the V-connectors.

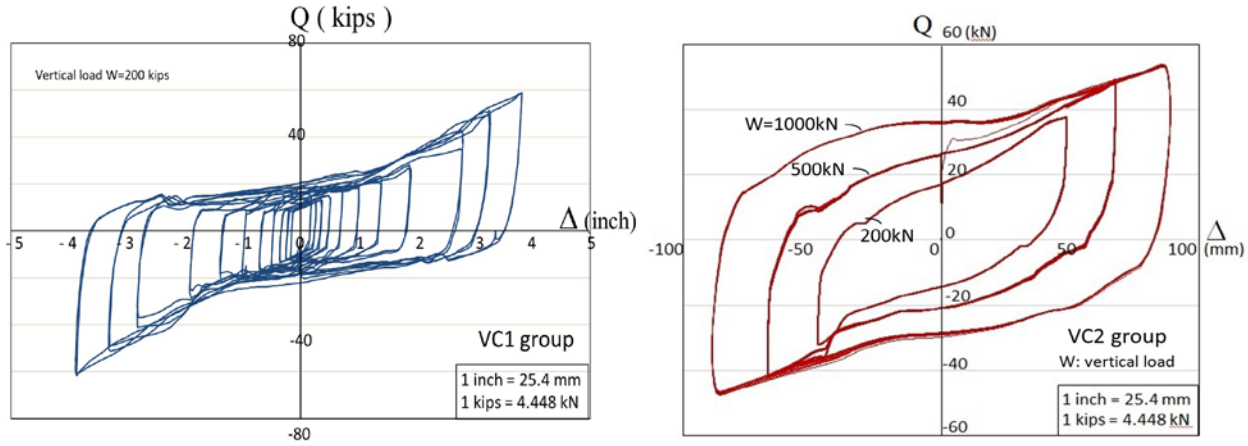

Fig. 29. Measured hysteresis behaviors for the two groups of V-connector specimens.

3.6.2 Comparison between the Two V-Connector Groups

For practical applications of the V-connectors, perhaps more useful results are those plotted in Fig. 30 that compare the two groups. For a hysteresis loop, such as that plotted in Fig. 29 or 30, the characteristic strength Q_d and the post-elastic stiffness K_d are the two major parameters that characterize the loop and determine the effective stiffness K_{eff} and thus the ductility factor R of an isolator. Q_d is mainly determined by the friction coefficient, as discussed above, whereas K_d reflects the stiffness of the SBP of a V-connector, as indicated in Fig. 3. The system's internal friction and rotation of the top block should also have a significant effect on elevating the slope of the hysteresis loop. Fig. 31 shows the results of rotation for VC1, which increases as the displacement increases. However, the initial stiffness is determined by the intrinsic structural properties of a V-connector. Therefore, the variation between K_{d0}^{VC1} and K_{d0}^{VC2} in Fig. 30 reflects mainly the differences between the geometries of the two groups of V-connectors and the properties listed in Table XI.

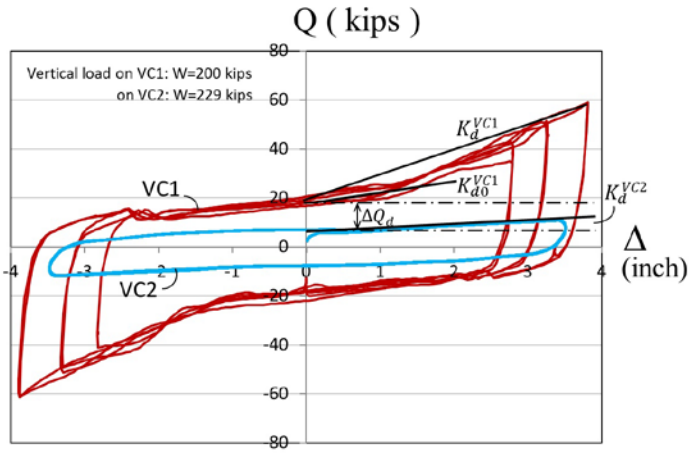

Fig. 30. Comparison of the measured hysteresis loops between the VC1 and VC2 product groups, where $K_{d0}^{VC1} \cong 10\ k/in$ and $K_{d0}^{VC2} \cong 2\ k/in$.

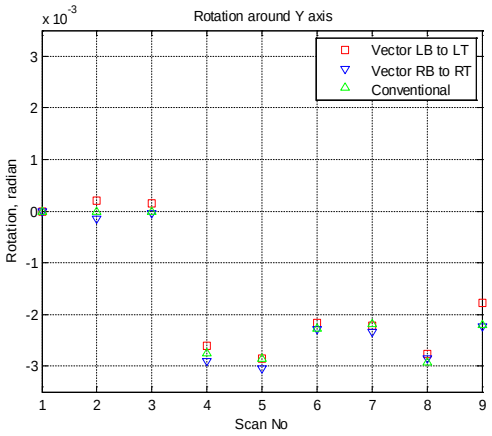

Fig. 31. Measured rotations for the top block of VC1 product-specimen group during displacement loading [13, 34].

3.6.3 Design Diagrams of V-connectors for Benchmark Bridges

The comparison in Fig. 30, in conjunction with the results in Fig. 29, provides a complementary understanding of how to modify the connector parameters to achieve better performance and which can be leveraged for practical design. Taking the AASHTO benchmark highway bridge as an example, a set of designs was obtained.

When an isolator is installed between a span bottom and a pier top, seismic protection comes from the capability of temporary separation to avoid the span's mass inertia affecting the entire structure that would cause the pier failure or move the span out of seat. When an isolator is able to prevent the span from shaking out of seat, it also assures the shear force and bending moment on the pier to be within the design allowances. The details of a desired design may vary as long as it meets these conditions. Presented in Figs. 32 and 33 are the design diagrams that give options for a 3-span benchmark bridge with even and uneven pier heights. Assuming a constant friction coefficient f_r = 0.05, the designs in the diagrams take the post-elastic stiffness K_d and the isolator's displacement capacity Δ_{iso} as the governing parameters to determine the corresponding shear force in the bridge pier, where the value of K_d is selected from the intervals indicated by Fig. 30 and Δ_{iso} refers to the predictions given by Fig. 12b. Similar diagrams can also be obtained for bending.

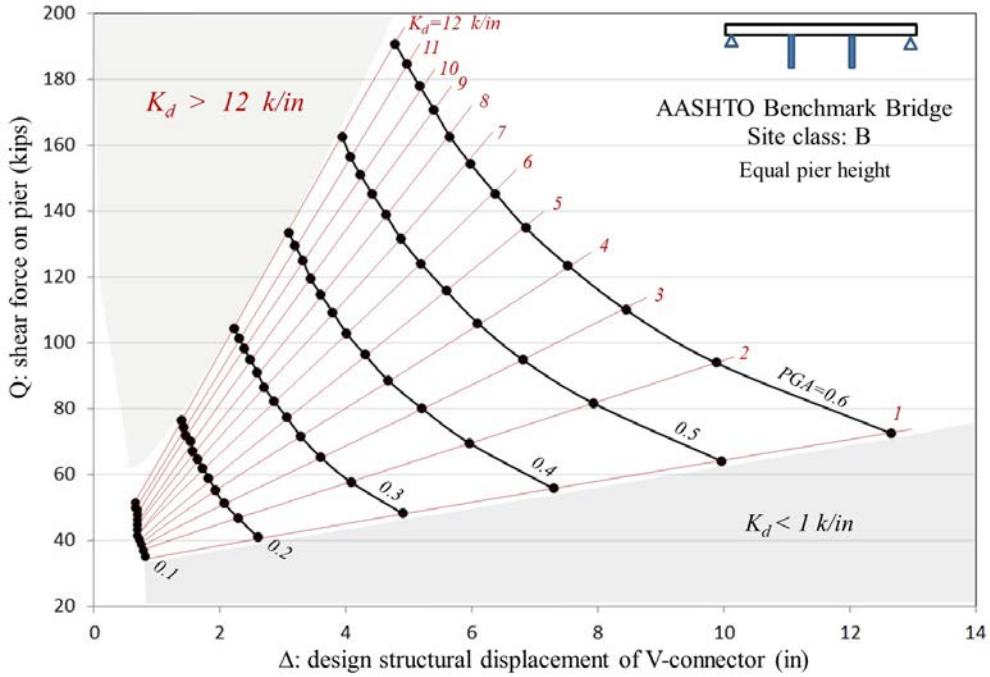

Fig. 32. Design diagram for the benchmark bridge in Fig. 1a with even pier heights under various PGA.

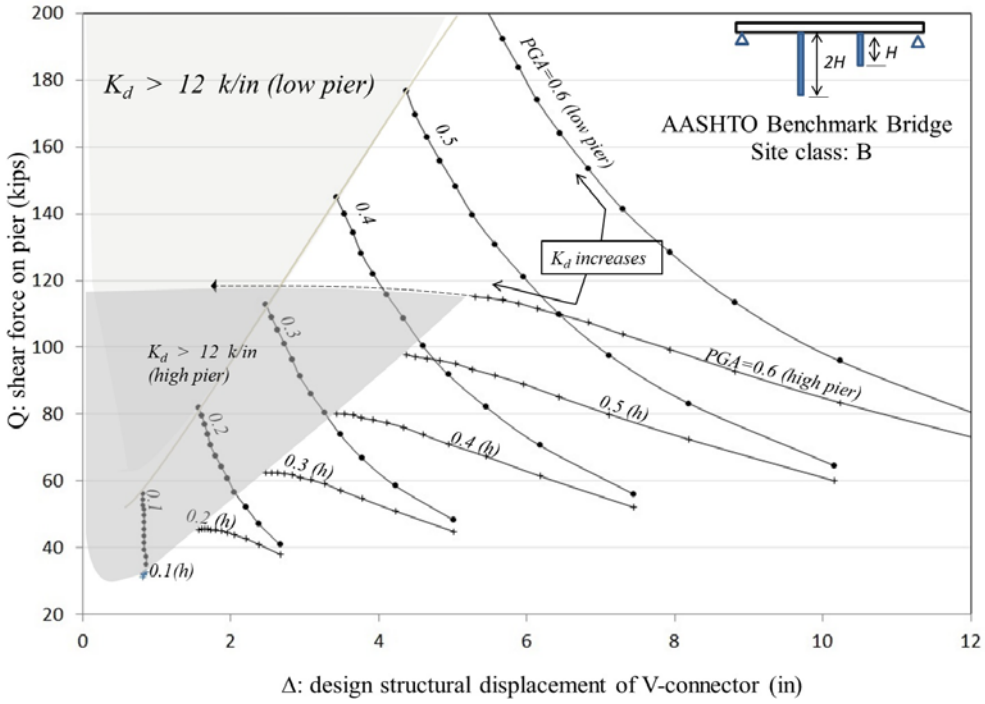

Fig. 33. Design diagram for the benchmark bridge in Fig. 1a with uneven pier heights under various PGA.

3.6.4 Safety Evaluation

A properly designed isolator should be able to keep a superstructure at its original position after the imposed load, such as an earthquake, passes, although slight deviation would be allowed if it is within the design allowance. However, one should be aware that the seismic design codes are generally based on probabilistic predictions. Statistically speaking, there is always a chance that a future earthquake could surpass the code's allowance. With this concern, the performance of the V-connectors under such situations was evaluated for safety assurance.

An experimental evaluation was conducted for a VC2 specimen by pushing the displacement beyond its design allowance to determine whether a dislocated movement, similar to the out-of-seat motion, would occur or the SBP would break.

Fig. 34 shows force-deformation loops for the VC2 specimen under the test. It is seen that a high resistance occurs that prevents the SBP's further lateral movement. This is because the imposed displacement has reached the tolerance of lateral separation provided by the V-crater, so the SBP is pushed until it is in full contact with the VGT's wall. Any further increase of lateral force pushed onto the upper block will be transferred into an uplift motion to the block that will slide along the SBP. In other words, no further shear force increase would be caused on the SBP and, instead, the forces acting onto the upper block would be transferred into compression onto the V-tube and the pier's concrete matrix through the SBP. This mechanism was shown by the computational results in Fig. 11, which predicted about 100% increase in failure load for the V-connector as compared to the instance without the V-shaped crater. In conclusion, for a bridge with appropriately designed V-connector, its capacity to prevent a beam from being shaken out of seat or the SBP's shear failure will be doubled as compared to the bridge with regular or conventional seismic-protection devices for the same intensity earthquake.

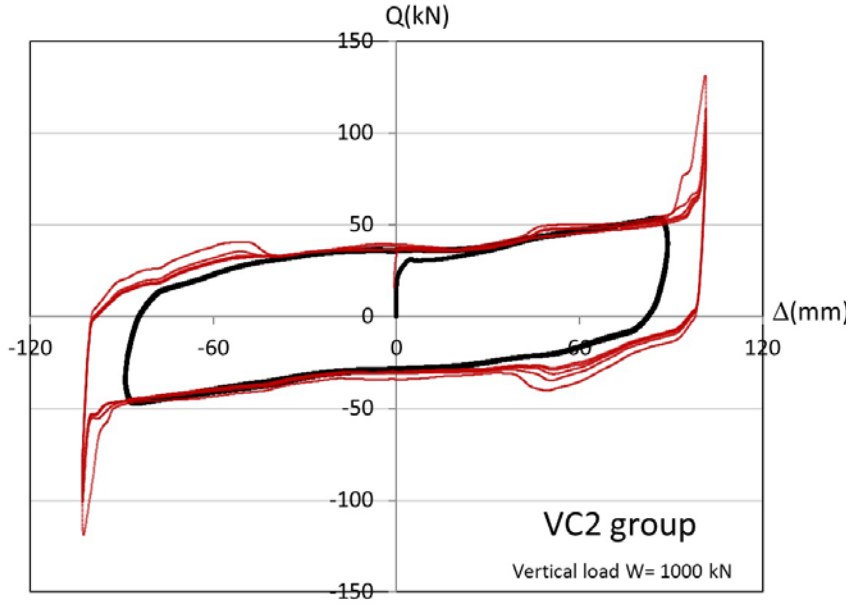

(a)

(b)

Fig. 34(a). Hysteresis loops when imposed lateral displacement has surpassed the design deformation capacity of a VC2 specimen; higher resistance presents when the pin is pushed to the side and touches the wall of the VGT; (b) the over-powered push left an indentation on the corner between the V tube and top pad while the hysteresis behavior is still on-going.

4. Summary and Conclusions

1. A systematic method that engages a theoretical model (Fig. 7a), a structural model (Fig. 7b), and finite element models (Figs. 9, 17a and 17b), was developed to investigate the performance of the V-connector system and the required design parameters.
2. The investigation identified that the "Single V-Tube Design" was more appropriate for conventional concrete and steel-girder bridges. With this design, two sub-classes of the V-connectors were developed -- Fix-End Pin Design (FP) and Hinged Pin Design (HP) (Fig. 20).
3. Two sets of HP V-connectors specimens were designed for the benchmark bridges (Figs. 1a and 1b) and tested simultaneously at the PEER laboratory of UC Berkeley and the Fengzhe Laboratory in China.
4. The measured results shown in Fig. 29 for the two groups of V-connector specimens at the two laboratories showed similar hysteresis behavior as predicted by the theoretical model (Fig. 3), verified the isolation function of the V-connector.
5. The test results shown in Fig. 34 demonstrated significant safety margin when the V-connector is over-pushed, i.e. a properly designed VGT could still protect under external force exceeding its design limit.
6. The test results verify and validate the V-connectors' capability to provide seismic isolation and assure safety, at least for the investigated short and middle span-length bridges shown in Figs. 1(a) and 1(b).

7. A group of design diagrams has been derived for actual application.

5. Plans for Implementation

The experiments conducted in this investigation appear to have verified and validated the V-connectors' capability for seismic isolation with considerable safety margin. Another uniqueness of V-connectors is their applicability for accelerated construction while assuring structural integrity and robustness. While scientific research is necessary to explore in depth the underlying physics and develop a more optimized design, the next step of this development will focus on working with bridge owners (states and local transportation authorities) to implement the V-connectors into the bridge design and developing codified industrial standard to guide engineering application.

For implementation of the V-connectors in highway infrastructure practice, the next step planned is to pursue developments particularly in the following two areas:

(i) Working with bridge owners, such as state and local transportation authorities, to inform them of the advantages of the V-connectors and seek their assistance/collaboration for implementing them into their respective bridge codes.
(ii) Working with conventional bearing vendors to standardize the V-connector product and the manufacturing process and raising funds for further development/refinement, if necessary.

6. Investigator's Profile

The P.I., Su Hao, obtained his Ph.D. degree from Zhejiang University in China and worked as a postdoctoral fellow at Tsinghua University in China and the Northwestern University in the United States. Before moving to the United States, he also worked as an engineer at the Gesellschaft für Kernenergieverwertung in Schiffbau und Schifffahrt (GKSS), a leading national laboratory in Germany. Dr. Hao has received several professional awards that include the Development Award in Hamburg, Germany, the Best Post-Presentation Award at the 10th European Conference on Fracture Mechanics, and the Merit Award by the Illinois Structural Engineers Association. Dr. Hao was also involved in an independent investigation of the 2007 Minneapolis I35W Bridge's collapse based on NTSB's material evidence. The investigation that was one step beyond official investigation [32, 33], revealed a general issue in the national bridge inventory.

7. References

[1] Presidential Executive Order 12996, 1990 January 5th of 1990
[2] Edward H. et. al, USGS Report, Feb. 2015, also, please refer to www.usgs.gov
[3] Schrank, D. and Lomax, T., 2005 Urban Mobility Report, Texas Transportation Institute.
[4] Hao, S., PCT/US2012/06312, "A Class of Bearings to Protect Structures from Earthquake and Other Similar Hazards", Nov. 2011
[5a] Hao, S., PCT/US2016/013741, "A Class of Seismic-Isolation Connectors Providing Robust Connection Close to Cast-in-Place While Enabling On-Site Assembling and Fast Construction for Bridges and Buildings", Jan. 2015.
[5b] Hao, S., US 14/989,725, "A Class of Seismic-Proof Connectors and Methods to Protect Buildings and Bridges from Earthquake Hazards and Fast Construction", Jan, 2016.
[6] Hao, S., PCT/US2018/013205, "A Class of Seismic-Isolation Connectors Providing Robust Connection Close to Cast-in-Place While Enabling On-Site Assembling and Fast Construction for Bridges and Buildings", Presentation in AFF50, TRB Annual Meeting at Washington DC, Jan, 11-17, 2017
[7] "LRFD Bridge Design Specifications", AASHTO, 6th Editions 1994 - 2017 and revisions.
[8] "Guide Specifications for Seismic Isolation Design", AASHTO, Third/Fourth Editions, 2010/2012
[9] "California Amendment to AASHTO LRFD Bridge Design Specifications – 4th Edition (Sec.14)"
[10] S. Hao, W. K. Liu. "Moving particle finite element with global super-convergence", Computer Method in Applied Mechanics and Engineering, Volume 196, Pages 6059-6072, 2006
[11] S. Hao, W. Liu, T. Belytschko, "Moving Particle Finite Element Method with Global Smoothness", Int. J. Numer. Methods Engineering, V.59, p.1007-1020, 2004
[12] S. Hao, W. K. Liu, G. B. Olson, B. Moran, " Multi-Scale Constitutive Model and Computational Framework for the Design of Ultra-High Strength, High Toughness Steels", Computer Method in Applied Mechanics and Engineering, Vol 193/17-20 pp 1865-1908, 2004.

[13] Shakhzod M. Takhirov, Khalid M. Mosalam, Yingjie Wu and Su Hao, “High Accuracy Structural Health Monitoring of Bridges with Terrestrial Laser Scanners: Validation in Laboratory and Field Conditions”, submitted for publication, 2018
[14] Federal Emergency Management Agency (FEMA), Report 461, “Interim Testing Protocols for Determining the Seismic Performance Characteristics of Structural and Nonstructural Components”, June 2007
[15] Federal Emergency Management Agency (FEMA), Reports 350-353, 2000
[16] Oden, J.T., Finite Elements of Nonlinear Continua. 1972, New York: McGraw-Hill Book Company.
[17] Hughes, T.J.R., The Finite Element Method. 1987, New Jersey: Prentice-Hall.
[18] Belytschko, T., Liu, W.K., and Moran, B., Nonlinear Finite Elements for Continua and Structures.2000, New York: John Wiley & Sons.
[19] Reddy, J. N., Mechanics of Laminated Composite Plates and Shells. Theory and Analysis, 2nd ed., CRC Press, Boca Raton, FL, 2004.
[20] Bathe K-J., Finite Element Procedure, Prentice-Hall Inc., 1996.
[21] ASCE/SEI, “Minimum Design Loads for Buildings and Other Structures”, 1995-2016 versions.
[22] Hao, S., Presentation at TRB 2016 Annual Meeting. Washington DC.
[23] “Experimental Investigation on the Seismic Response of Bridge Bearings”, Univ. of California, Berkeley, EERC-2008-02, 2008.
[24] Bazant, B. “Stability of Structures: Elastic, Inelastic, Fracture, and Damage Theories”, Mineola, Dover Pub. 2001
[25] Lee, G. C., Tong, M. and Dong, T. (2004). “On Design of Highway Bridges against Unintentional Hazards and Hazards and Malicious Attacks.” Proc. US-Japan Workshop on Bridge Engineering, Washington, D.C., October 4-6, 2004.
[26] Frangopol, D. et al. "Multi-criteria Optimization of Life-Cycle Maintenance Programs using Advanced Modeling and Computational Tools", Chapt. 1 in “Trends in Civil and Structural Computing”, Saxe-Coburg Publications, 2009
[27] S. Hao, Strom, Brandon, Gordon, Grant; Krishnaswamy, Sridhar; Achenbach, Jan, “Scattering of the Lowest Lamb Wave Modes by a Corrosion Pit”, Research in Nondestructive Detection, 22, Oct., 2011.
[28] S. Hao, H. Lin, R Robert Binomiemic, D. M.G. Combsd and G. Fett, “A multi-scale model of intergranular fracture and computer simulation of fracture toughness of a carburized steel”, J. Computational Materials Science, Volume 48, Issue 2, 2010, pp.241-249
[29] S. Hao, Q. Wang, M. L. Keer, “A Mechanical Approach to Solve Two-Dimensional Static Electrical and Magnetic Fields: Applications to Contact between Conductors under Electrical Load”, J. Applied Mechanics, ASME Trans., Volume 77, May, 2010, 031013.
[30] S. Hao, M. L. Keer, “Rolling Contact between Rigid Cylinder and Semi-infinite Elastic Body with Sliding and Adhesion”, J. Tribology, ASME Trans. Volume 129, Pages 481-494, 2007
[31] S. Hao, W. K. Liu, G. B. Olson, B. Moran, “ Multi-Scale Constitutive Model and Computational Framework for the Design of Ultra-High Strength, High Toughness Steels”, Computer Method in Applied Mechanics and Engineering, Vol 193/17-20 pp 1865-1908, 2004
[32] Hao, S., “I-35W Bridge Collapse”, J. Bridge Engineering, Issue 5, 2010, pp.608-618
[33] Hao, S., “I-35W Bridge Collapse – Lessons Learned and Challenges Revealed”, Int. J. Forensic Engineering, Vol. 2, 2014, pp.21-67.
[34] TRB NCHRP 12-68, Final Report
[35] Wu, Yingjie, Ph. D. Student by Professor Mosalam of UC Berkeley.